NASA Technical Memorandum 78615

Effect of Tip Planform on Blade Loading Characteristics for a Two-Bladed Rotor in Hover

John D. Ballard, Kenneth L. Orloff,
and Alan B. Luebs

November 1979

National Aeronautics and
Space Administration

NASA Technical Memorandum 78615

Effect of Tip Planform on Blade Loading Characteristics for a Two-Bladed Rotor in Hover

John D. Ballard
Kenneth L. Orloff, Ames Research Center, Moffett Field, California
Alan B. Luebs, Gates Lear Corp., Wichita, Kansas

National Aeronautics and
Space Administration

Ames Research Center
Moffett Field, California 94035

EFFECT OF TIP PLANFORM ON BLADE LOADING CHARACTERISTICS FOR A TWO-BLADED ROTOR IN HOVER

John D. Ballard, Kenneth L. Orloff

Ames Research Center

and

Alan B. Luebs

Gates Lear Corp., Wichita, Kansas

SUMMARY

A laser velocimeter was used to study the flow surrounding a 2.13-m-diam, two-bladed, teetering model-scale helicopter rotor operating in the hover condition. The rotor system employed interchangeable blade tips over the outer 25% radius. A conventional rectangular planform and an experimental ogee tip shape were studied. The radial distribution of the blade circulation was obtained by measuring the velocity tangent to a closed rectangular contour around the airfoil section at a number of radial locations. A relationship between local circulation and bound vorticity is invoked to obtain the radial variations in the sectional lifting properties of the blade. The tip vortex-induced velocity was also measured immediately behind the generating blade and immediately before the encounter with the following blade. The mutual influences between blade loading, shed vorticity, and the structure of the encountered vortex are quantified by the results presented and are discussed comparatively for the rectangular and ogee planforms. The experimental loading for the rectangular tip is also compared with predictions of existing rotor analysis.

INTRODUCTION

Rotorcraft hover performance is influenced by the radial variations of the rotor-induced velocity field (refs. 1, 2). For a given rotor configuration and operating condition, the designer can influence this induced-velocity distribution through the choice of radial distributions of blade chord, twist, and airfoil section. The precise manner in which these design parameters affect the induced velocities has not yet been completely explained. A number of discrete numerical procedures have been developed that model the individual blade wakes and predict the rotor inflow and blade loading (refs. 3, 4). Unfortunately, most of the data available for validation of techniques have been restricted to total rotor lift and loading distributions. Thus, the discrepancies between measured and predicted rotor performance (total thrust and

torque) have been attributed to an assortment of nonlinear or three-dimensional effects and to inaccuracies in the specification of the vortex wake. What has been lacking is a precise experimental description of the rotor-induced flow field and the associated vortex wake geometry. Prior to the advent of the laser velocimeter (LV), it was not possible to nonintrusively generate such a quantitative description.

Many previous attempts to measure the detailed structure of the rotor-induced velocity flow field have employed flow-field-intrusive instruments (refs. 5, 6). The extent to which the sensitive vortex flow field is modified by probe interference leaves some question as to the quality of the resulting data. On the other hand, the laser velocimeter can accurately measure flow-field velocities without itself disturbing the flow (refs. 7, 8). Using an LV, researchers have been able to measure vortex position, velocity profiles, rotor-generated local circulation, and the flow associated with a vortex-blade encounter (refs. 9-11). However, an accurate experimental assessment of the manner in which the wake structure shed by a preceding blade influences the characteristics of the radial distribution of lift on the following blade, has not been available.

The radial distribution of lift is significantly influenced by the proximity of the vortex wake from the preceding blade passage. The velocity distribution of the encountered vortex has a significant influence on the inflow patterns experienced by the blade, and subsequently on the overall performance of the rotor. It is conjectured that a significant improvement can be realized in rotor blade efficiency by tailoring the blade-tip planforms. This tailoring can have a twofold influence. First, the vortex roll-up process is altered (ref. 12) to generate a more diffuse vortex whose circulation remains the same as for a rectangular planform but is distributed over a larger region, thereby increasing core size and reducing maximum rotational velocities. Second, when a following blade with this modified planform encounters the more diffuse vortex, the character of the interaction is such that loading gradients and the ensuing undesirable vibrations are reduced with an attendant improvement in performance. Accordingly, this paper presents the results of an experiment in which a laser velocimeter was used to measure flow-field velocities in close proximity to a blade of a hovering rotor, including measurements of the bound circulation and hence the sectional lift. The influence of a change in rotor blade-tip shape (rectangular to ogee) on the vortex roll-up phenomena and the influence of the modified wake on the radial loading distribution have also been experimentally documented.

NOTATION

b number of blades

C_e thrust effective chord, cm, $\dfrac{\int_0^1 cx^2\,dx}{\int_0^1 x^2\,dx}$

C_ℓ local lift coefficient, $\frac{\ell}{(\rho/2)c_e(\Omega r)^2}$

c local blade chord, cm

$\bar{c}$ mean geometries chord, cm, $\int_0^R \frac{c\ dr}{R}$

D_x total distance increment along a chordwise traverse

D_z total distance increment along vertical traverse

L total rotor lift, N, $\frac{\rho}{2} bc_e\Omega^2 \int_0^R r^2 C_\ell\ dr$

ℓ rotor blade loading per unit length, N/m, $\frac{\rho}{2} c(\Omega r)^2 C_\ell$

$\vec{\ell}$ distance vector of closed rectangular traverse around airfoil, cm

R rotor radius, m

r local radial position, m

S_1 measured circulation along forward vertical traverse

S_2 measured circulation along top horizontal traverse

S_3 measured circulation along rear vertical traverse

S_4 measured circulation along lower horizontal traverse

U_z vertical component of velocity; positive upward, m/sec

x distance chordwise from blade leading edge; positive aft, m

x_1 distance chordwise from blade quarter-chord; positive toward the airfoil leading edge, m

y distance radially; positive radially outward from hub, m

z distance vertical from chord line of blade tip; positive up, m

Γ circulation $\oint \vec{v} \cdot d\vec{\ell}$

$\theta_{0.75}$ blade pitch angle at 0.75R, deg

θ_{TW} blade twist angle relative to 0.75R, deg

$\vec{v}$ velocity vector tangent to $\vec{\ell}$, m/sec

ρ air density, kg/m^3

$\bar{\sigma}$ rotor solidity referenced to mean geometric chord, $\frac{b\bar{c}}{\pi R}$

σ rotor solidity referenced to thrust effective chord, $\frac{bc_e}{\pi R}$

ψ vortex age, deg

Ω rotor rotational speed, rad/sec

ROTOR, TEST CONDITIONS, AND PROCEDURES

A hovering, two-bladed teetering model-scale rotor with interchangeable tips was used for this investigation. The rotor characteristics and operating conditions are presented in tables 1 and 2, respectively. The rotor hub had been used in a previous study (ref. 11). Rotor blade construction necessitated the low rotational speed. Figure 1 is a photograph of the rotor operating with the laser beams projected at a point in the rotor inflow. The rotor blade characteristics and the two tip shapes studied (rectangular and ogee) are shown in figures 2 and 3. Table 3 presents the ogee chord distribution.

TABLE 1.- GEOMETRIC BLADE PROPERTIES

Parameter	Tip planform	
	Rectangular	Ogee
Rotor hub precone, α	1.5°	1.5°
Number of blades, b	2	2
Rotor radius, R	1.05 m	1.05 m
Blade twist, θ_{TW}	see fig. 2	see fig. 2
Airfoil	NACA 0012	NACA 0012
Flapping hinge undersling	0.0086R	0.0086R
Reference blade chord	7.62 cm	7.62 cm
Mean geometric chord, $\bar{c}$	7.62 cm	7.22 cm
Thrust effective chord, c_e	7.62 cm	6.477 cm
Rotor solidity, $\bar{\sigma} = \frac{b\bar{c}}{\pi R}$	0.0464	0.0440
$\sigma = \frac{bc_e}{\pi R}$	0.0464	0.0396
Root cut out, X_{co}	13.4% R	13.4% R

TABLE 2.- TEST OPERATING CONDITIONS

Parameter	Tip planform	
	Rectangular	Ogee
Rotor speed, Ω	73.3 rad/sec	73.3 rad/sec
Air density, ρ	Standard atmospheric conditions	Standard atmospheric conditions
Collective pitch, $\theta_{0.75}$	9.8°	9.8°
Tip Reynolds number, $Re_{1.0}$	4×10^5	4×10^5
Tip speed, ΩR	76.6 m/sec	76.6 m/sec
Thrust coefficient to solidity ratio, C_t/σ	0.099	0.099

TABLE 3.- OGEE BLADE TIP PLANFORM COORDINATES

Radial blade station, r/R	Chord, cm	Radial blade station, r/R	Chord, cm
0.75	7.62	0.94	4.48
.80	7.62	.95	3.43
.85	7.62	.96	2.40
.90	7.62	.97	1.47
.91	7.39	.98	0.88
.92	6.38	.99	.49
.93	5.54	1.00	.0

The laser velocimeter used to make the present measurements had been used in earlier studies (refs. 11-13). The addition of directional sensitivity for both components of velocity was implemented in this test. The vertical and chordwise components of the flow-field velocity were measured at the laser focal volume (i.e., the point where the beams intersect). Rotor flow-field surveys were made by incrementally traversing the LV focal volume along the x, y, or z coordinate and obtaining the chordwise and vertical velocity components. At each radial location, the local blade circulation was determined by measuring the velocity component tangent to a closed rectangular contour around the airfoil section (ref. 13). For steady-state flow (blade-referenced coordinates in hover) this measured circulation is related to the bound vorticity, and subsequently to the section lift coefficient according to:

$$\frac{\Gamma}{\Omega(R)^2} = \oint \frac{\vec{v}}{\Omega R} \cdot \frac{d\vec{\ell}}{R}$$

$$C_\ell = \frac{2\Gamma}{(\Omega r)c}$$

Data samples were transferred to the minicomputer processing and control system only during an acceptance time of 60 μsec after the blade had reached the prescribed azimuth (ref. 13). This time corresponds to a blade rotation of 0.25°, representing a blade movement at the tip of 6% of the chord and a corresponding lesser amount at inboard radial locations.

The instantaneous mean velocity at each point is taken to be the ensemble average of 20 data samples. The fidelity to which this ensemble average approximates the true instantaneous velocity is highly dependent on the reproducibility of the flow field at a fixed phase of rotor rotation (ref. 14). To improve the reproducibility, both rotor rotation speed and blade flapping angle were monitored and were required to be within prescribed limits (±0.5° blade flapping angle and ±0.2 rad/sec rotational speed). For conditions outside these limits, data transfer to the computer was inhibited. For data samples that obey Student's T statistics, and for a flow that is reproducible to within 7% (combined aperiodicity and turbulence intensity), 20 velocity samples yield a 90% confidence level that the ensemble average is the correct mean with less than 3% error. All velocities presented herein are these ensemble averages normalized by rotor-tip speed (ΩR).

Because it is difficult to assure an exactly reproducible periodic flow on a day-to-day basis, the accuracy in the measurements of the circulation is given based on repeatability rather than absolute velocity measurement accuracy. In this respect, the circulation values were found to have a long-time repeatability of better than 95%.

The circulation was determined at a sufficient number of radial locations to accurately represent the radial distribution of circulation. An example of the real-time data output format is presented in figure 4. Traverses were also made radially to document the structure of the vortex wake in both the roll-up region and after approximately 180° of rotation just before encountering the following blade.

RESULTS

For both the rectangular and ogee tip configurations, the circulation was measured about a closed rectangular contour enclosing each local blade radial station. The velocity distributions within the tip vortex roll-up region were measured close behind the blade tip and just before the tip vortex passed beneath the following blade. The measured distributions (circulation, trailing vortex velocity at $\psi = 0°$, and trailing vortex velocity at $\psi = 180°$) are presented in figures 5 and 6, respectively, for the rectangular tip configuration. The peak circulation is located at a radial station of 0.90 (see fig. 5). From that position out to the tip, the steep gradient observed in the circulation distribution indicates a concentration of the shed vorticity. That concentration is apparent in the velocity profile shown in figure 6(a), in which the vorticity is centered at an approximate radial station of 0.98.

After 180° of rotor azimuth displacement (fig. 6(b)), this trailing vortex has been displaced radially inward to a radial station of 0.86R, which represents the wake contraction. This velocity structure also demonstrates the extent to which the vorticity has diffused outward from the vortex center. In the region of the vortex center, scatter in the vortex velocity profile data, taken at the same blade radial station, is evident and is an indication of the inflow variations between velocity samples.

Measured distributions of circulation and trailing vortex velocity are presented for the ogee tip configuration in figures 7 and 8. The peak circulation value is at a radial station of 0.85 and the gradient of the radial circulation (fig. 7) is clearly less than the gradient near the tip for the rectangular blade. This reduction in gradient is also evident in the more diffuse distribution of vorticity behind the blade (fig. 8(a)), with a nominal center of vorticity at a radial station of 0.93. After 180° of rotor azimuth displacement, the trailing vortex has been displaced radially to a station of 0.82R and is less concentrated than for the rectangular tip (fig. 8(b)).

The section lift coefficient and loading distributions are obtained from the circulation distribution by the following expressions:

$$C_{\ell} = \frac{2\Gamma/R^2\Omega}{(r/R)(c/R)}$$

$$\frac{\ell}{\rho\Omega^2R^3} = \frac{r}{R}\frac{\Gamma}{\Omega R^2}$$

The radial distribution of the loading and lift coefficient for the rectangular tip is given in figures 9 and 10; the distribution for the ogee configuration is given in figures 11 and 12.

DISCUSSION AND COMPARISON WITH THEORY

The operating conditions (blade collective pitch and rotational speed) were chosen to be the same for both tip shapes. As a result, the rectangular tip configuration produced 114 N of lift and the ogee configuration produced 101 N. Hence, although the ogee planform had 15% less weighted blade solidity (based on thrust effective chord), it produced 11% less lift. The above values for lift were determined by integrating the loading distribution:

$$L = b\int_0^R \ell \, dr$$

for both the rectangular tip configuration (fig. 9) and the ogee tip configuration (fig. 11). Measurements were not made over the inboard portion of the span ($r/R < 0.40$) because of experimental limitations. Hence, to compute

the total lift, these loading distributions were extrapolated inward to the blade cutout section by selecting a distribution that was in agreement with analytical predictions.

Figure 9 also shows, for the rectangular tip configuration, two different analytical methods that were used to generate loading distributions. The vortex-line method uses strip theory to devise an analytically defined vortex wake and to predict blade loading. The empirically prescribed wake method uses lifting surface theory with an empirically prescribed discrete vortex wake. The defined wake geometry constitutes the major difference between the two predicted results for blade loading. The vortex-line technique uses rotor momentum to predict the wake geometry, and the empirically prescribed wake method was used with the Landgrebe Wake Model (ref. 2). Although both methods predict an increased loading near the tip, the magnitudes are less than the experimental value. However, the empirically prescribed wake model predicts a peak loading and a radial distribution that in the vicinity of the tip is in better agreement with the experimental distributions than the results obtained from the vortex-line model.

For the ogee configuration loading distribution (fig. 11), it is noted that the position of the peak loading is located farther inboard than for the rectangular tip. Also, there is a substantial reduction in loading over the outer 10% of the blade radius; this reduction is a reflection of the ogee planform. The radially inward displacement of the loading peak is partly the direct result of the ogee planform and is also indirectly due to the tip vortex of the preceding blade, which for the ogee tip is generated farther inboard (fig. 8(a)) than for the rectangular tip (fig. 6(a)).

The above loading distributions were computed from the bound circulation distribution for the rectangular (fig. 5) and ogee configurations (fig. 7). For the ogee configuration, the location of the peak circulation occurs farther inboard by approximately 5.5% of the radius than the peak for the rectangular tip. The amplitude of the peak circulation is nearly the same for both tip shapes, but for the ogee tip there is a reduction in radial gradient outboard of the peak and there is a substantial reduction in magnitude near the tip. However, the distributions of the circulation in the vicinity of the tip (from approximately 0.25R inboard to approximately 0.06R outboard of the peak), are nearly identical for the two configurations.

With the above noted characteristics of the circulation distribution, trailing vorticity generated by the ogee shape is expected to be significantly more diffuse than for the rectangular tip. This is evident in the induced-velocity distributions measured aft of the trailing edge (figs. 6(a) and 8(a) for the rectangular and ogee tips, respectively). With the ogee tip, the tip vortex is farther inboard by about 0.04R, both at $\psi = 0°$ and $\psi = 180°$; hence, both the bound circulation and the wake vorticity have been displaced inboard. For the rectangular tip, this velocity distribution resembles that of a concentrated vortex; for the ogee tip the velocity distribution suggests a more diffuse distribution of vorticity, as expected. Because the circulation peak values are the same for both the ogee and rectangular tip configurations, the total strength of the trailed vorticity generated by each should be the same;

this is so even though the ogee configuration may have a larger core diameter and different distributions of vorticity and velocity through the core. If this is true, then outside the region of rotational flow the induced velocities should closely approach those of the concentrated vortex generated by the rectangular tip. This is substantiated by the similar distributions about the circulation peak, which is significantly influenced by the encountered tip vortex shed from the preceding blade.

The radial distributions of bound vorticity (circulation) were used to determine the radial C_ℓ distributions that are presented in figures 10 and 12 for the rectangular and ogee configurations, respectively. As expected, the primary peak in the C_ℓ distribution for the ogee tip configuration is located farther inboard than for the rectangular configuration. There are, however, other notable differences between the two configurations. First, for the ogee tip there is a secondary peak farther outboard near the tip that is not apparent for the rectangular tip. This peak is thought to be the result of the self-induced upwash generated (due to the ogee shape) by the blade's own shed vorticity inboard of the tip. That upwash is evident in the velocity distributions near the trailing edge of the ogee tip (fig. 8(a)). In contrast, the primary peak for both the ogee and rectangular tips is the result of the upwash portion of the induced velocity distribution from the tip vortex of the preceding blade (figs. 6(b) and 8(b), respectively). The radial location of the encountered vortex, correlates well with the variation in C_ℓ that it induces on the blade. The slightly greater magnitude of the general ogee tip C_ℓ distribution relative to that of the rectangular tip is the result of the inboard shift of the tip vortex generated by the ogee tip. The induced velocity field of the ogee tip vortex is also moved inboard such that when combined with the lower tangential velocities (Ωr) the blade experiences an increased induced angle of attack, and hence an increased C_ℓ.

Lastly, for the rectangular tip configuration, there is a dip in the C_ℓ distribution at a radial station of 0.60. This dip ($\Delta C_\ell = 0.04$) corresponds to a $\Delta\alpha$ of 0.4°; this measured effect was found to be repeatable. Although there has been much speculation, no adequate explanation is available.

Figures 13 through 70 present the flow-field velocities tangent to a closed rectangular contour around the airfoil; hence, the measured bound circulation for both planform shapes, as a function of blade radial station. Table 4 is a list of the figures.

TABLE 4.- LIST OF FIGURES

Figure no.	Title
Figure 1.-	Photograph of laser velocimeter and rotor in hover condition.
Figure 2.-	Basic rotor blade geometry.
Figure 3.-	Photograph of rectangular and ogee blade-tip planforms.
Figure 4.-	Typical real-time presentation of data during circulation measurement.
Figure 5.-	Measured bound circulation for rectangular blade tip.
Figure 6.-	Wake velocity radial distribution for rectangular blade tip.
Figure 7.-	Measured bound circulation for ogee blade tip.
Figure 8.-	Wake velocity radial distribution for ogee blade tip.
Figure 9.-	Blade section loading for rectangular blade tip.
Figure 10.-	Lift coefficient radial distribution for rectangular blade tip.
Figure 11.-	Blade section loading for ogee blade tip.
Figure 12.-	Lift coefficient radial distribution for ogee blade tip.
	Circulation Measurements for Rectangular Blade Tip
Figure 13.-	Flow-field velocities about circulation contour at blade radial station 0.549R for rectangular blade tip.
Figure 14.-	Flow-field velocities about circulation contour at blade radial station 0.574R for rectangular blade tip.
Figure 15.-	Flow-field velocities about circulation contour at blade radial station 0.598R for rectangular blade tip.
Figure 16.-	Flow-field velocities about circulation contour at blade radial station 0.599R for rectangular blade tip.
Figure 17.-	Flow-field velocities about circulation contour at blade radial station 0.623R for rectangular blade tip.
Figure 18.-	Flow-field velocities about circulation contour at blade radial station 0.648R for rectangular blade tip.

TABLE 4.- CONTINUED

Figure no.	Title
Figure 19.-	Flow-field velocities about circulation contour at blade radial station 0.699R for rectangular blade tip.
Figure 20.-	Flow-field velocities about circulation contour at blade radial station 0.748R for rectangular blade tip.
Figure 21.-	Flow-field velocities about circulation contour at blade radial station 0.750R for rectangular blade tip.
Figure 22.-	Flow-field velocities about circulation contour at blade radial station 0.774R for rectangular blade tip.
Figure 23.-	Flow-field velocities about circulation contour at blade radial station 0.775R for rectangular blade tip.
Figure 24.-	Flow-field velocities about circulation contour at blade radial station 0.779R for rectangular blade tip.
Figure 25.-	Flow-field velocities about circulation contour at blade radial station 0.798R for rectangular blade tip.
Figure 26.-	Flow-field velocities about circulation contour at blade radial station 0.799R for rectangular blade tip.
Figure 27.-	Flow-field velocities about circulation contour at blade radial station 0.799R for rectangular blade tip.
Figure 28.-	Flow-field velocities about circulation contour at blade radial station 0.823R for rectangular blade tip.
Figure 29.-	Flow-field velocities about circulation contour at blade radial station 0.825R for rectangular blade tip.
Figure 30.-	Flow-field velocities about circulation contour at blade radial station 0.848R for rectangular blade tip.
Figure 31.-	Flow-field velocities about circulation contour at blade radial station 0.849R for rectangular blade tip.
Figure 32.-	Flow-field velocities about circulation contour at blade radial station 0.873R for rectangular blade tip.
Figure 33.-	Flow-field velocities about circulation contour at blade radial station 0.875R for rectangular blade tip.

TABLE 4.- CONTINUED

Figure no.	Title
Figure 34.-	Flow-field velocities about circulation contour at blade radial station 0.880R for rectangular blade tip.
Figure 35.-	Flow-field velocities about circulation contour at blade radial station 0.899R for rectangular blade tip.
Figure 36.-	Flow-field velocities about circulation contour at blade radial station 0.899R for rectangular blade tip.
Figure 37.-	Flow-field velocities about circulation contour at blade radial station 0.910R for rectangular blade tip.
Figure 38.-	Flow-field velocities about circulation contour at blade radial station 0.923R for rectangular blade tip.
Figure 39.-	Flow-field velocities about circulation contour at blade radial station 0.948R for rectangular blade tip.
Figure 40.-	Flow-field velocities about circulation contour at blade radial station 0.949R for rectangular blade tip.
Figure 41.-	Flow-field velocities about circulation contour at blade radial station 0.960R for rectangular blade tip.
Figure 42.-	Flow-field velocities about circulation contour at blade radial station 0.965R for rectangular blade tip.
Figure 43.-	Flow-field velocities about circulation contour at blade radial station 0.975R for rectangular blade tip.
Figure 44.-	Flow-field velocities about circulation contour at blade radial station 0.980R for rectangular blade tip.
Figure 45.-	Flow-field velocities about circulation contour at blade radial station 0.990R for rectangular blade tip.
Figure 46.-	Flow-field velocities about circulation contour at blade radial station 0.999R for rectangular blade tip.
Figure 47.-	Flow-field velocities about circulation contour at blade radial station 1.003R for rectangular blade tip.

TABLE 4.- CONTINUED

Figure no.	Title
	Circulation Measurements for Ogee Blade Tip
Figure 48.-	Flow-field velocities about circulation contour at blade radial station 0.398R for ogee blade tip.
Figure 49.-	Flow-field velocities about circulation contour at blade radial station 0.501R for ogee blade tip.
Figure 50.-	Flow-field velocities about circulation contour at blade radial station 0.550R for ogee blade tip.
Figure 51.-	Flow-field velocities about circulation contour at blade radial station 0.600R for ogee blade tip.
Figure 52.-	Flow-field velocities about circulation contour at blade radial station 0.649R for ogee blade tip.
Figure 53.-	Flow-field velocities about circulation contour at blade radial station 0.700R for ogee blade tip.
Figure 54.-	Flow-field velocities about circulation contour at blade radial station 0.724R for ogee blade tip.
Figure 55.-	Flow-field velocities about circulation contour at blade radial station 0.751R for ogee blade tip.
Figure 56.-	Flow-field velocities about circulation contour at blade radial station 0.775R for ogee blade tip.
Figure 57.-	Flow-field velocities about circulation contour at blade radial station 0.800R for ogee blade tip.
Figure 58.-	Flow-field velocities about circulation contour at blade radial station 0.800R for ogee blade tip.
Figure 59.-	Flow-field velocities about circulation contour at blade radial station 0.816R for ogee blade tip.
Figure 60.-	Flow-field velocities about circulation contour at blade radial station 0.825R for ogee blade tip.
Figure 61.-	Flow-field velocities about circulation contour at blade radial station 0.834R for ogee blade tip.
Figure 62.-	Flow-field velocities about circulation contour at blade radial station 0.848R for ogee blade tip.

TABLE 4.- CONCLUDED

Figure no.	Title
Figure 63.-	Flow-field velocities about circulation contour at blade radial station 0.865R for ogee blade tip.
Figure 64.-	Flow-field velocities about circulation contour at blade radial station 0.876R for ogee blade tip.
Figure 65.-	Flow-field velocities about circulation contour at blade radial station 0.901R for ogee blade tip.
Figure 66.-	Flow-field velocities about circulation contour at blade radial station 0.925R for ogee blade tip.
Figure 67.-	Flow-field velocities about circulation contour at blade radial station 0.948R for ogee blade tip.
Figure 68.-	Flow-field velocities about circulation contour at blade radial station 0.974R for ogee blade tip.
Figure 69.-	Flow-field velocities about circulation contour at blade radial station 0.990R for ogee blade tip.
Figure 70.-	Flow-field velocities about circulation contour at blade radial station 1.000R for ogee blade tip.

CONCLUDING REMARKS

A remote-measuring, nonintrusive velocity probe, such as the laser velocimeter, has been shown to be an effective way of examining the instantaneous inflow and vortex wake structures of a hovering model-scale rotor. The exact location of the center of the vortex filament and the details of the velocity distribution were measured with sufficient accuracy to indicate vortex decay rate from vortex inception (ψ = 0°) to blade-vortex encounter (ψ = 180°) for a two-bladed rotor. Moreover, closed-loop velocity surveys were conducted from which the radial loading distribution could be determined. The loading distributions for the rectangular and ogee tip configurations confirm the utility of the experimental approach. Indeed, subtle variations in radial distributions of lift can now be measured with sufficient sensitivity and repeatability to provide an accurate data base for the validation of numerical predictions that are designed to predict blade loading and subsequently rotorcraft performance.

REFERENCES

1. Landgrebe, A. J.; and Cheney, M. C.: Rotor Wakes — Key to Performance Prediction. Presented at the Symposium on Status of Testing and Modeling Techniques for V/STOL Aircraft, Oct. 1972.

2. Landgrebe, A. J.: The Wake Geometry of a Hovering Helicopter Rotor and Its Influence on Rotor Performance. Presented at the 28th Annual National Forum of The American Helicopter Society, Washington, D.C., May 1972.

3. Scully, M. P.: A Method of Computing Helicopter Vortex Wake Distortion: M. I. T. Aeroelastic and Structures Research Laboratory, ASRL TR-138-1, June 1967.

4. Landgrebe, A. J.; and Egolf, T. A.: Prediction of Helicopter Induced Flow Velocities Using the Rotorcraft Wake Analysis. Presented at the 32nd Annual National V/STOL Forum of the American Helicopter Society, Washington, D.C., May 1976.

5. Chigier, N. A.; and Corsiglia, V. R.: Tip Vortices Velocity Distributions. Presented at the 27th Annual National Forum of the American Helicopter Society, Washington, D.C., May 1971.

6. Boatwright, D.: Measurements of Velocity Components in the Wake of a Full-Scale Helicopter Rotor in Hover. USAAMRDL TR-72-33, Aug. 1972.

7. Landgrebe, A. J.; and Johnson, B. V.: Measurements of Model Helicopter Rotor Flow Velocities with a Laser Doppler Velocimeter. Tech. Note, J. American Helicopter Soc., vol. 19, no. 2, July 74.

8. Sullivan, J. P.: An Experimental Investigation of Vortex Rings and Helicopter Wakes Using a Laser Doppler Velocimeter. M. I. T. Aerophysics Laboratory TR-183, June 1973.

9. Orloff, K. L.: The Spanwise Lift Distribution on a Wing from Flowfield Velocity Surveys. Presented at the AIAA 11th Fluid and Plasma Dynamics Conference, Seattle, Wash., July 1978.

10. Biggers, J. C.; and Orloff, K. L.: Laser Velocimeter Measurements of the Helicopter Rotor — Induced Flow Fields. J. American Helicopter Soc., vol. 20, no. 1, Jan. 1975.

11. Biggers, J. C.; Lee, A.; Orloff, K. L.; and Lemmer, O. J.: Measurements of Helicopter Rotor Tip Vortices. Presented at the 33rd Annual National Forum of the American Helicopter Society, Washington, D.C., May 1977.

12. Piziali, R.; and Trenka, A.: An Experimental Study of Blade Tip Vortices. Cornell Aeronautical Laboratory, NASA CR-66860, Jan. 1970.

13. Biggers, J. C.; Chu, S.; and Orloff, K. L.: Laser Velocimeter Measurements of a Rotor Blade Loads and Tip Vortex Rollup. Preprint No. 900, 31st Annual National Forum of the American Helicopter Society, Washington, D.C., May 1975.

14. Orloff, K. L.: Laser Doppler Anemometer Diagnostics in Unsteady Flow. Proceedings of the Dynamic Flow Conference, 1978, Baltimore, Md., Sept. 18-21, 1978.

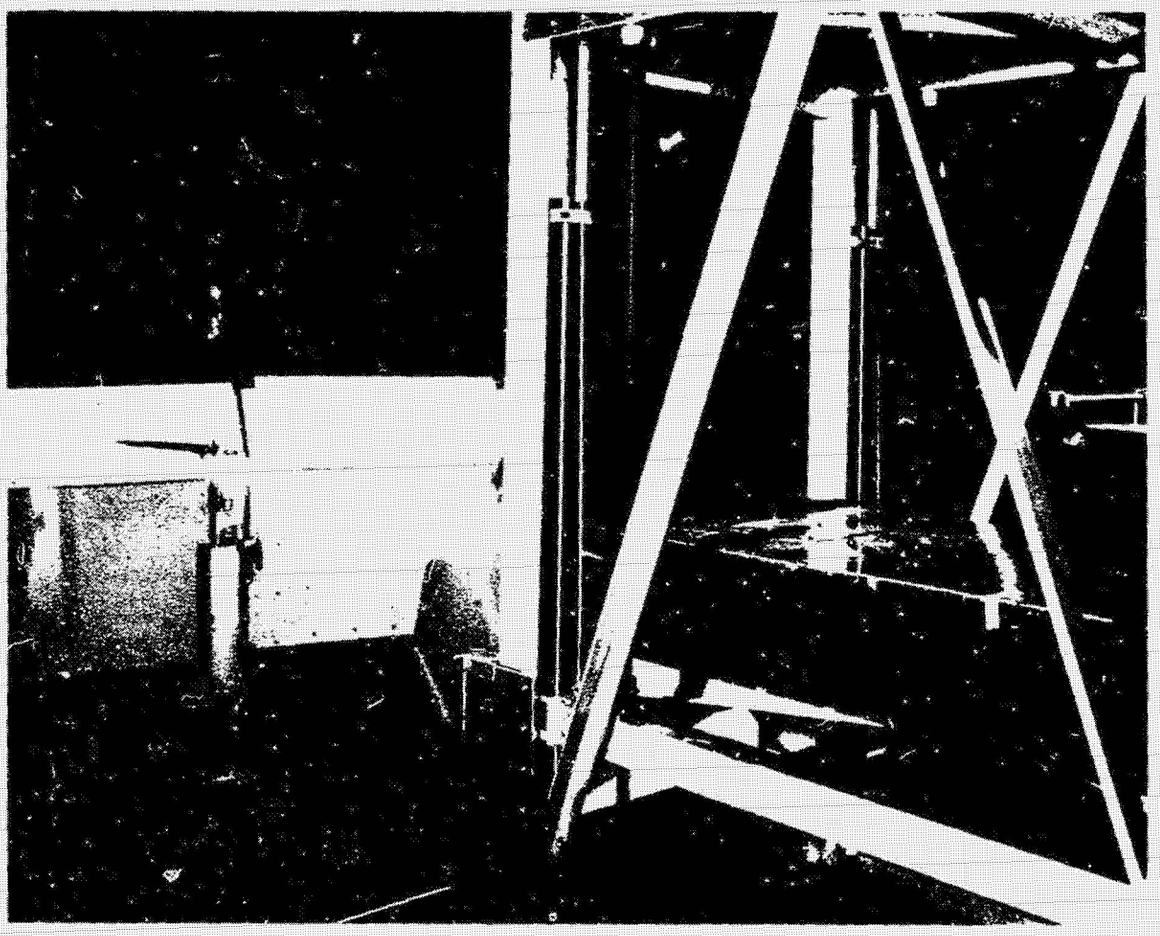

Figure 1.- Photograph of laser velocimeter and rotor in hover condition.

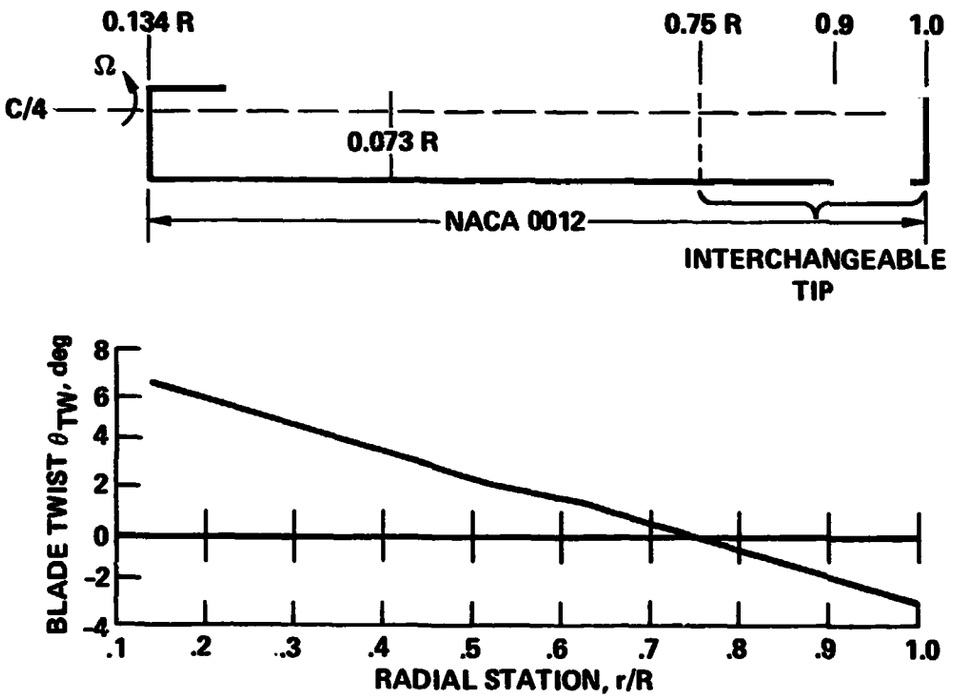

Figure 2.- Basic rotor blade geometry.

Figure 3.- Photograph of rectangular and ogee blade-tip planforms.

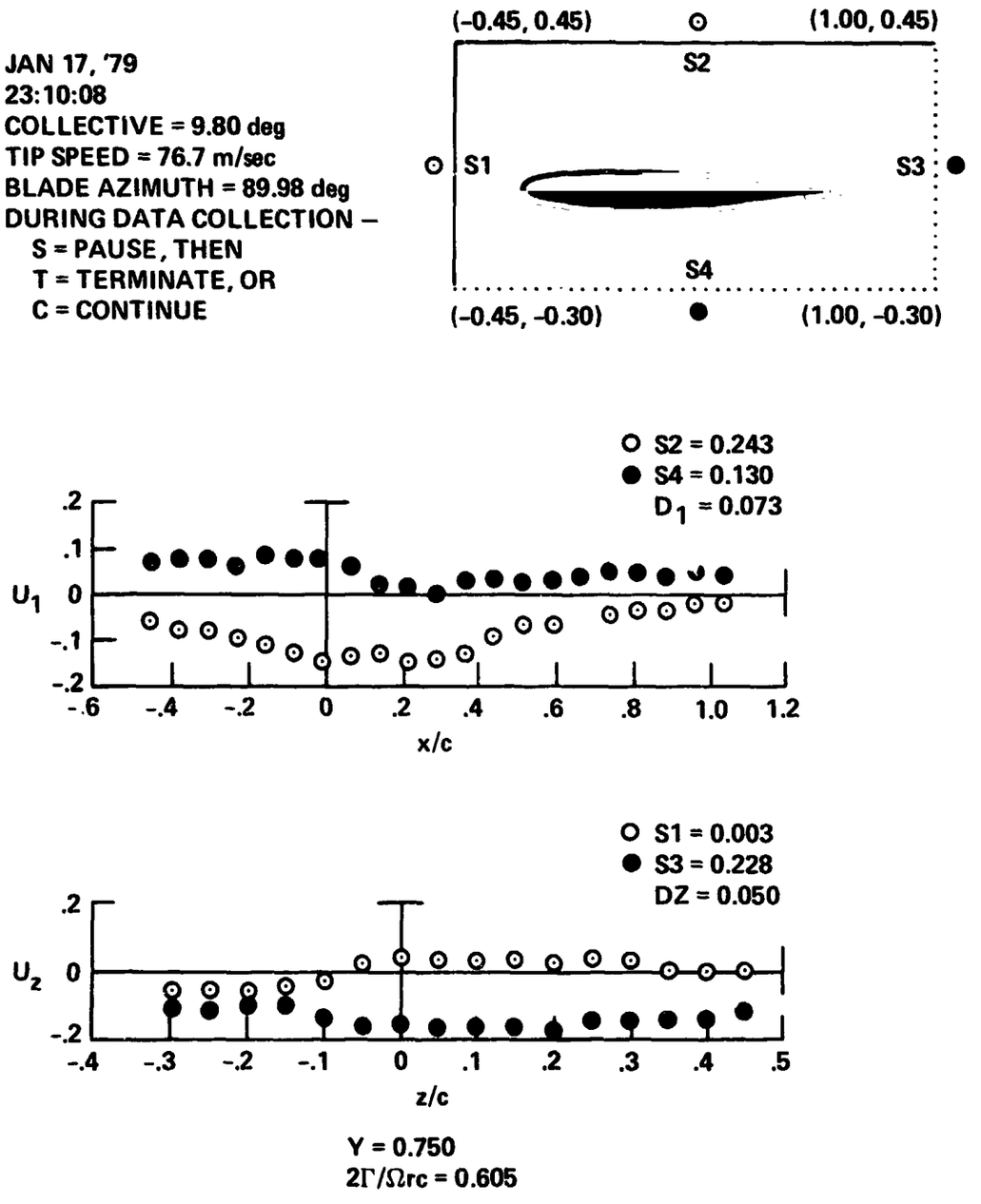

Figure 4.- Typical real-time presentation of data during circulation measurement.

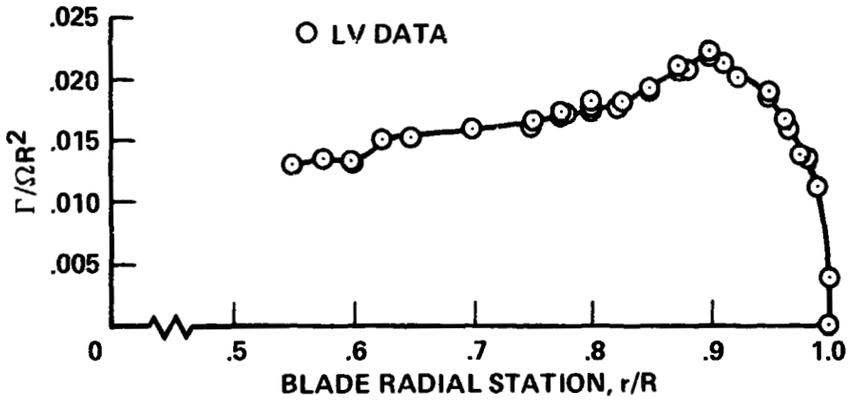

Figure 5.- Measured bound circulation for rectangular blade tip.

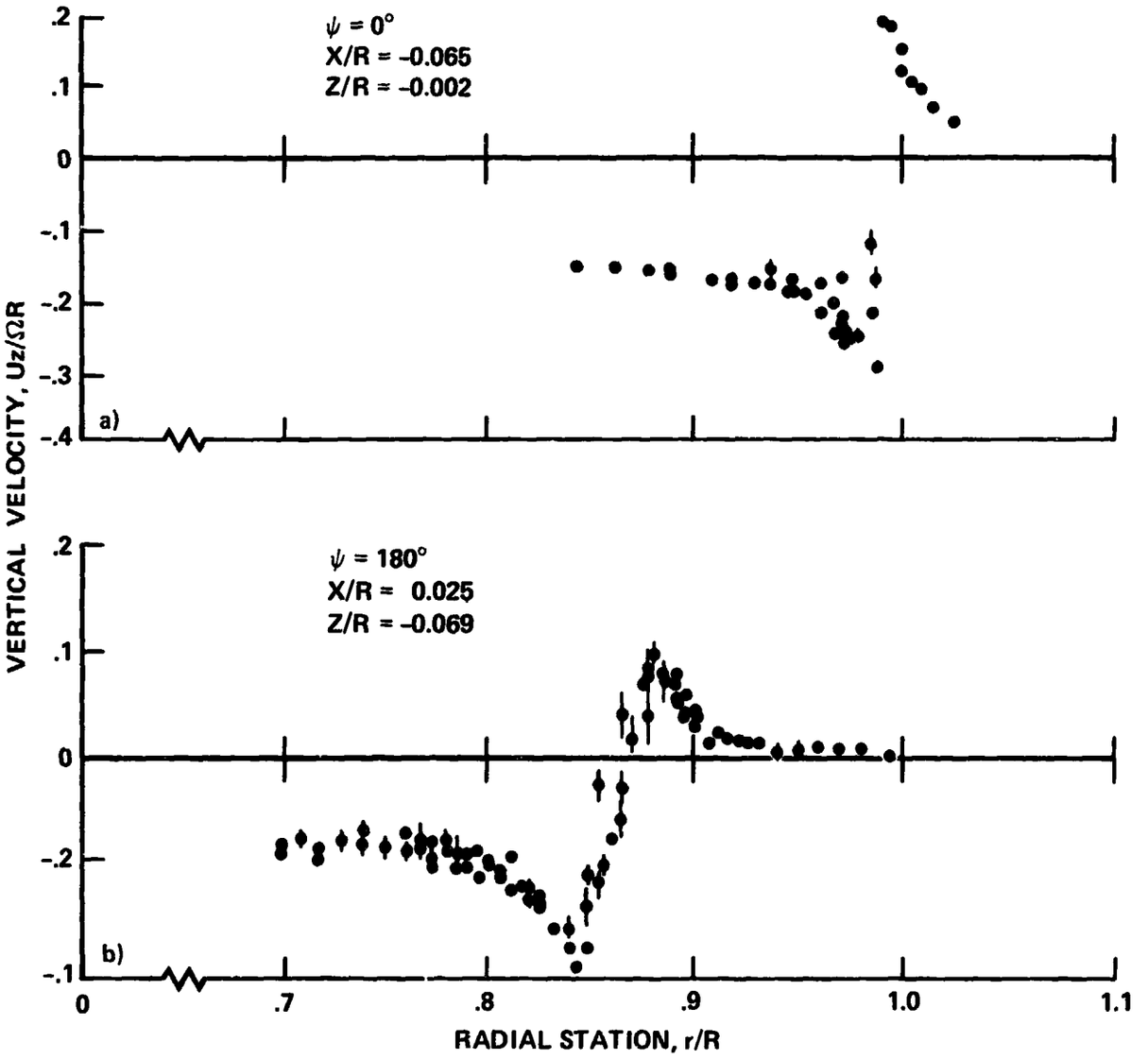

(a) Vertical velocity at generating blade (ψ = 0°).

(b) Vertical velocity at encounter with following blade (ψ = 180°).

Figure 6.- Wake velocity radial distribution for rectangular blade tip.

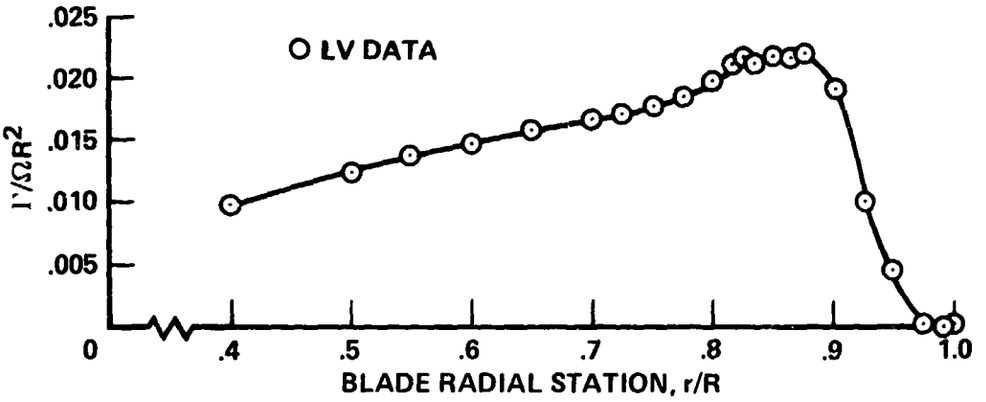

Figure 7.- Measured bound circulation for ogee blade tip.

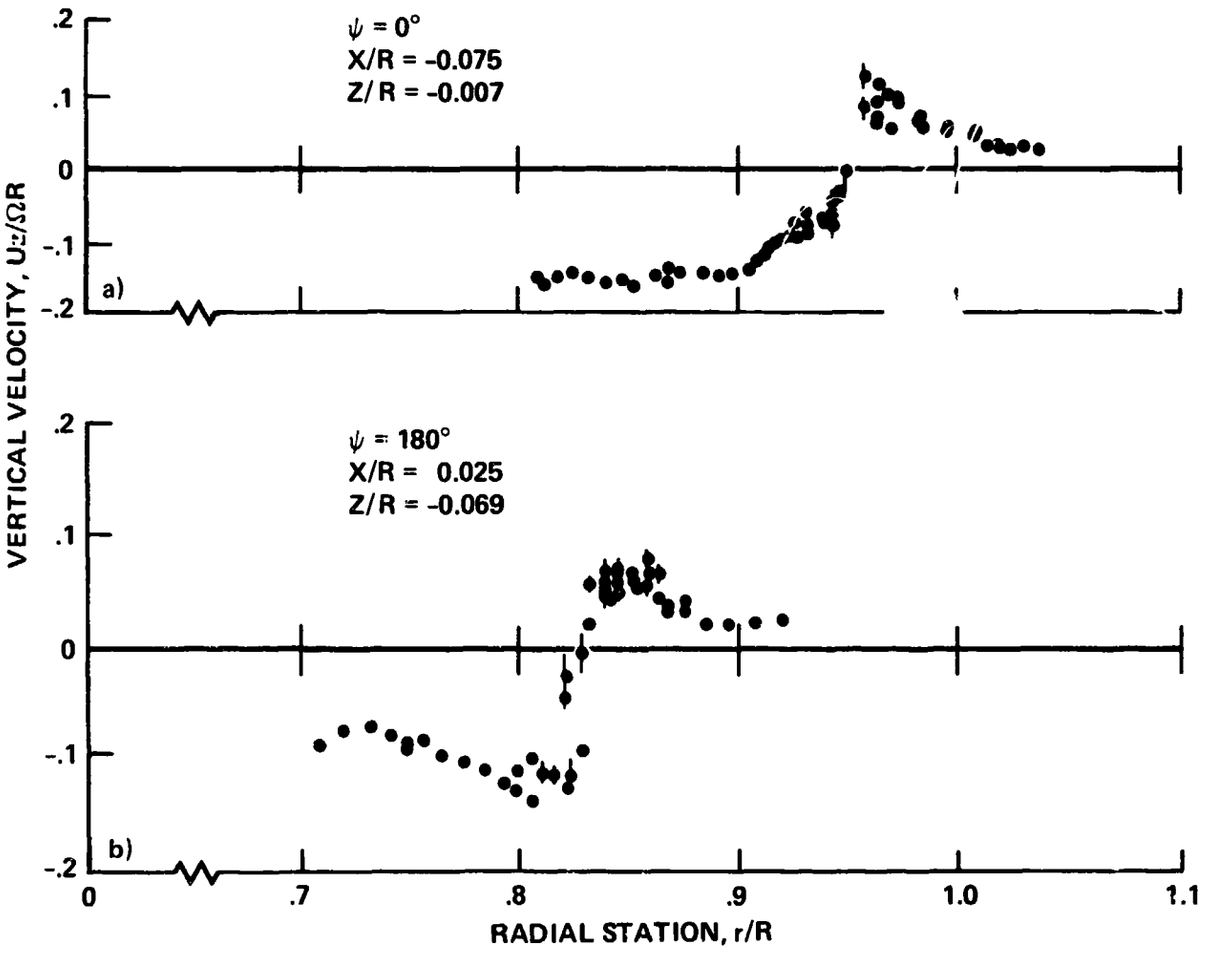

(a) Vertical velocity at generating blade (ψ = 0°).

(b) Vertical velocity at encounter with following blade (ψ = 180°).

Figure 8.- Wake velocity radial distribution for ogee blade tip.

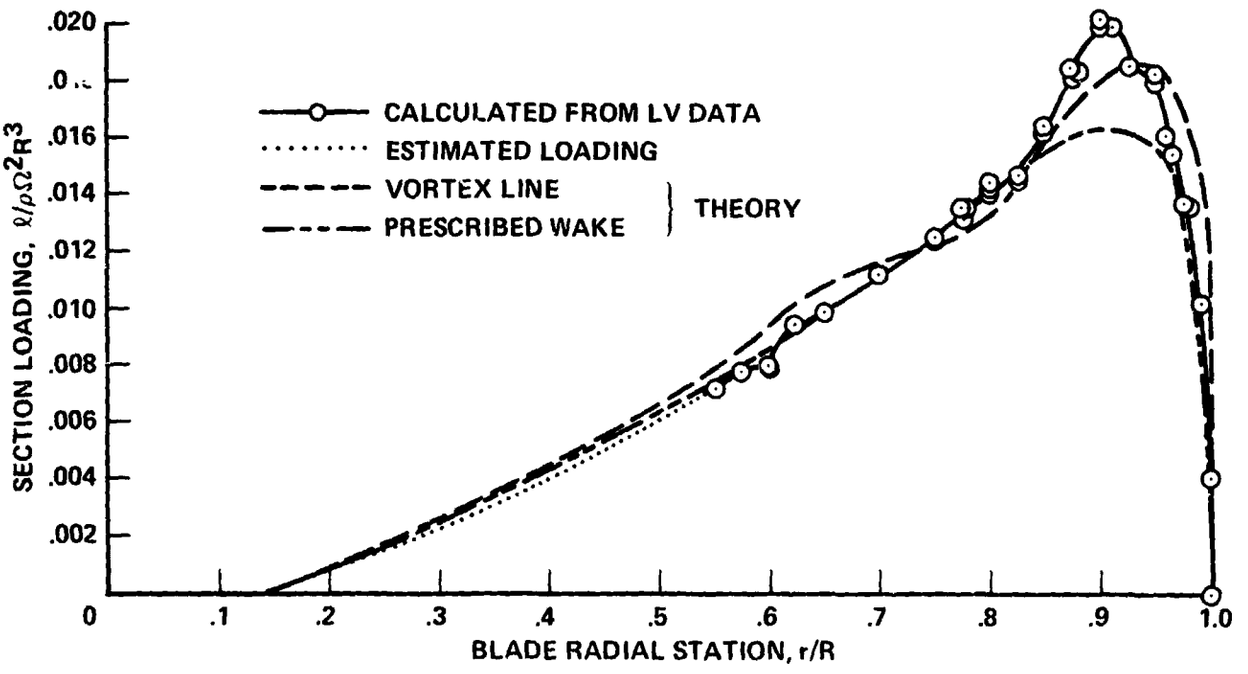

Figure 9.- Blade section loading for rectangular blade tip.

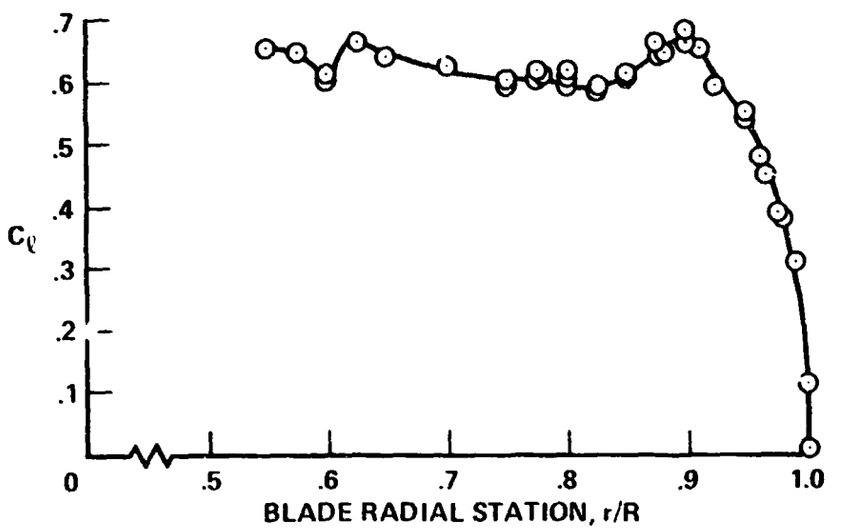

Figure 10.- Lift coefficient radial distribution for rectangular blade tip.

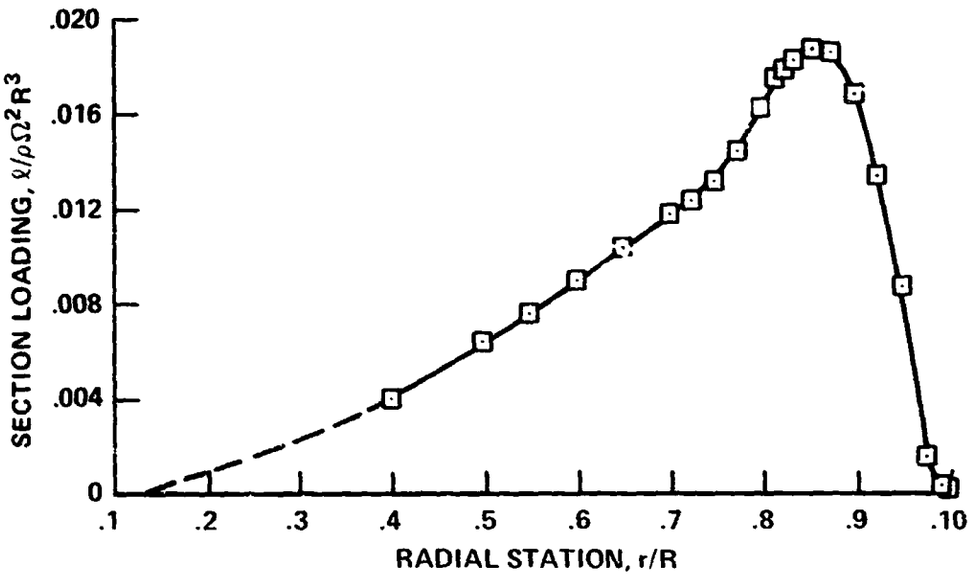

Figure 11.- Blade section loading for ogee blade tip.

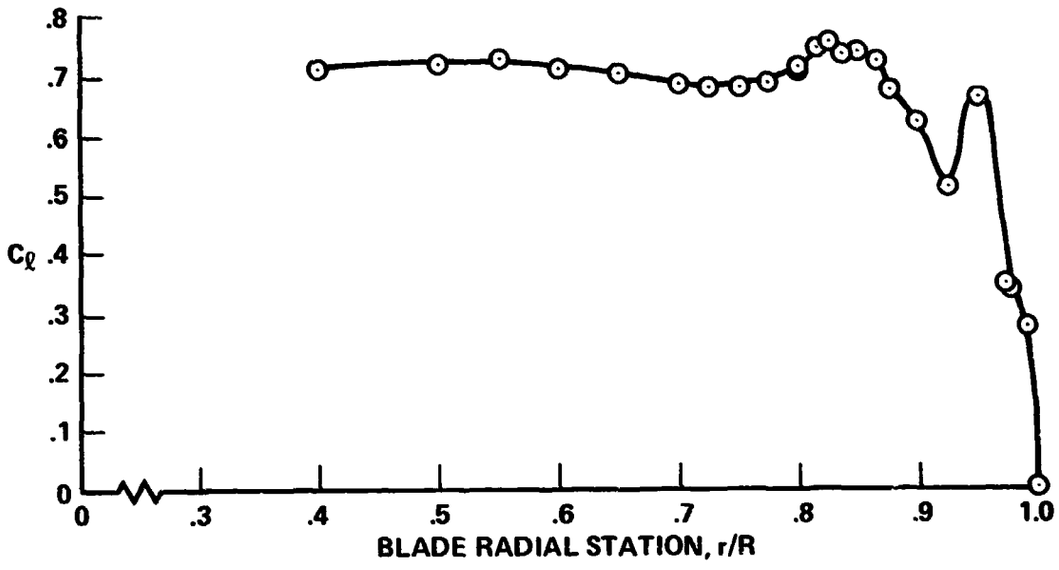

Figure 12.- Lift coefficient radial distribution for ogee blade tip.

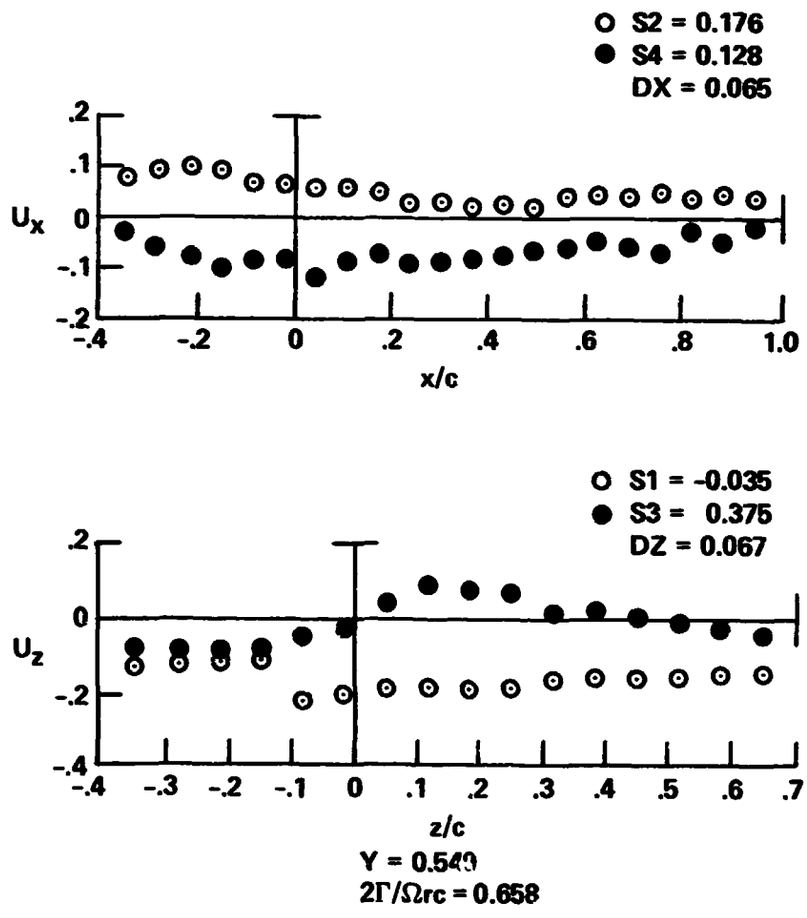

Figure 13.- Flow-field velocities about circulation contour at blade radial station 0.549R for rectangular blade tip.

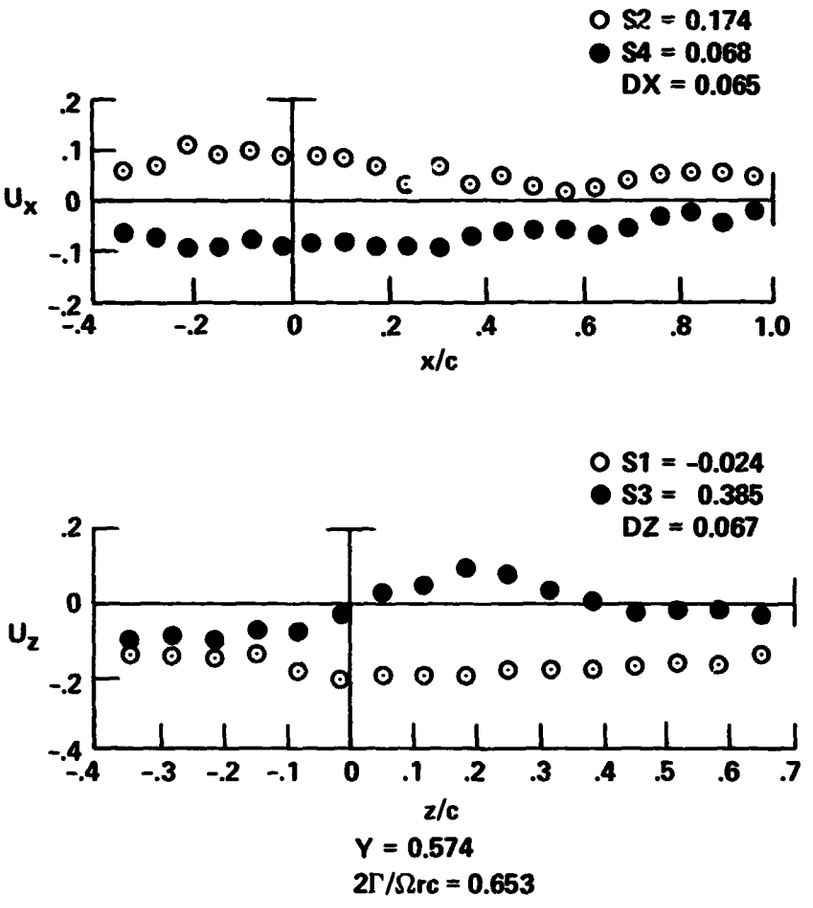

Figure 14.- Flow-field velocities about circulation contour at blade radial station 0.574R for rectangular blade tip.

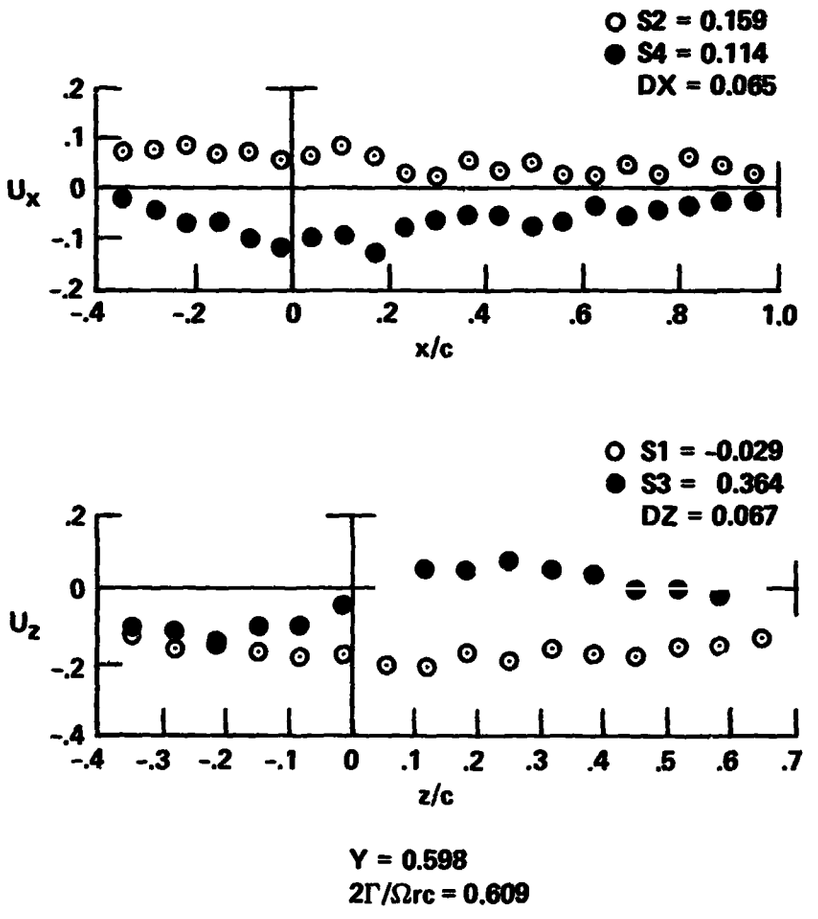

Figure 15.- Flow-field velocities about circulation contour at blade radial station 0.598R for rectangular blade tip.

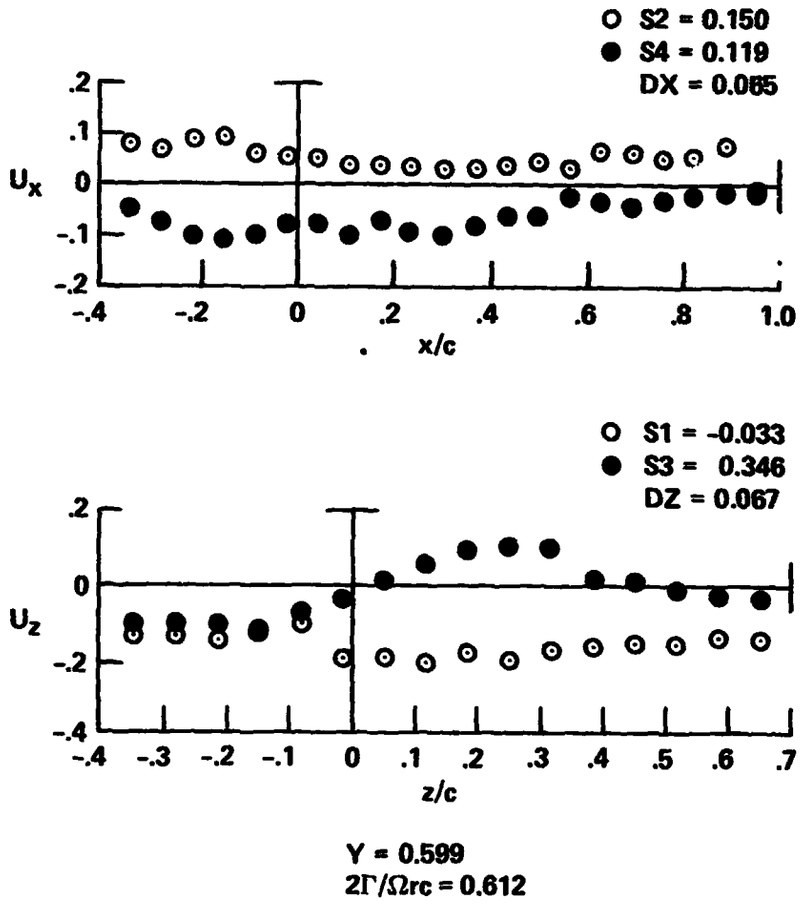

Figure 16.- Flow-field velocities about circulation contour at blade radial station 0.599R for rectangular blade tip.

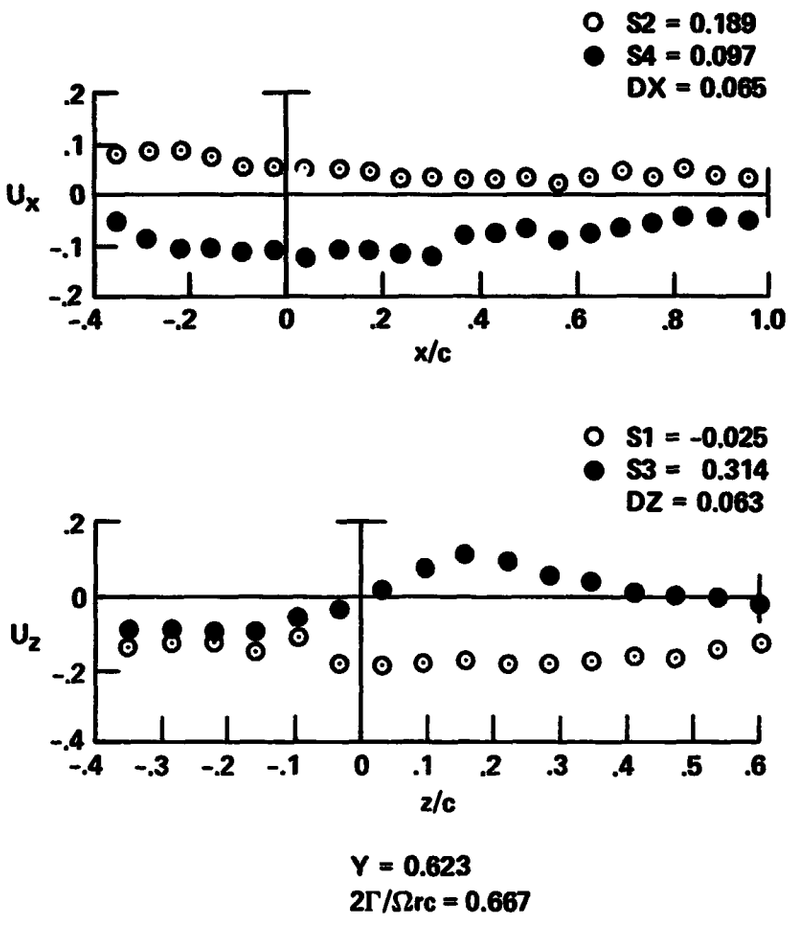

Figure 17.- Flow-field velocities about circulation contour at blade radial station 0.623R for rectangular blade tip.

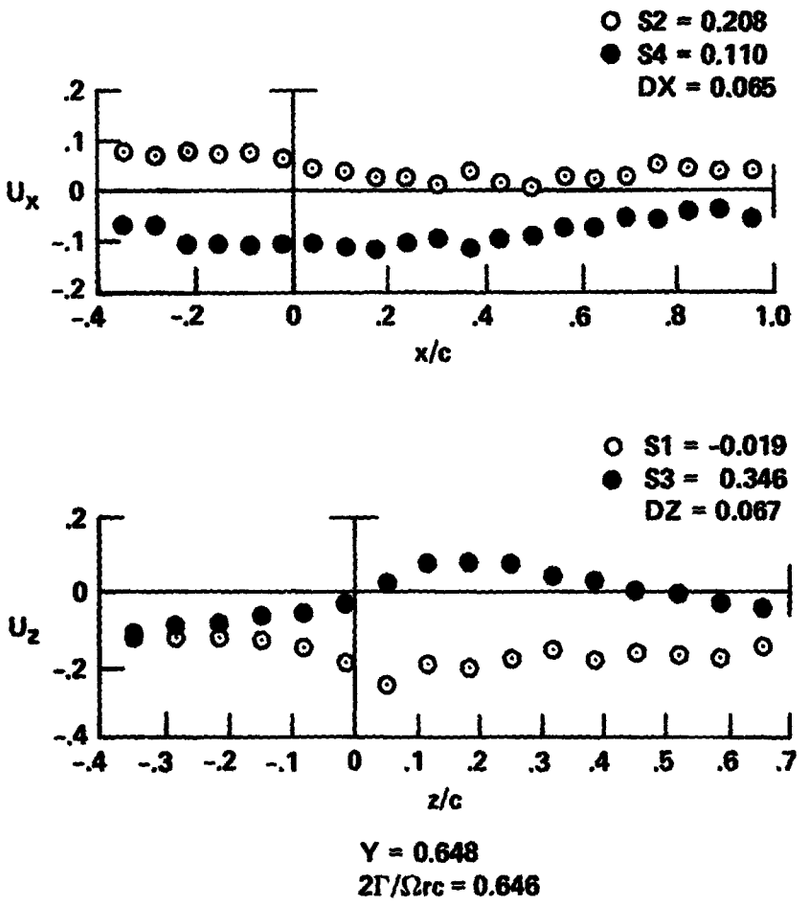

Figure 18.- Flow-field velocities about circulation contour at blade radial station 0.648R for rectangular blade tip.

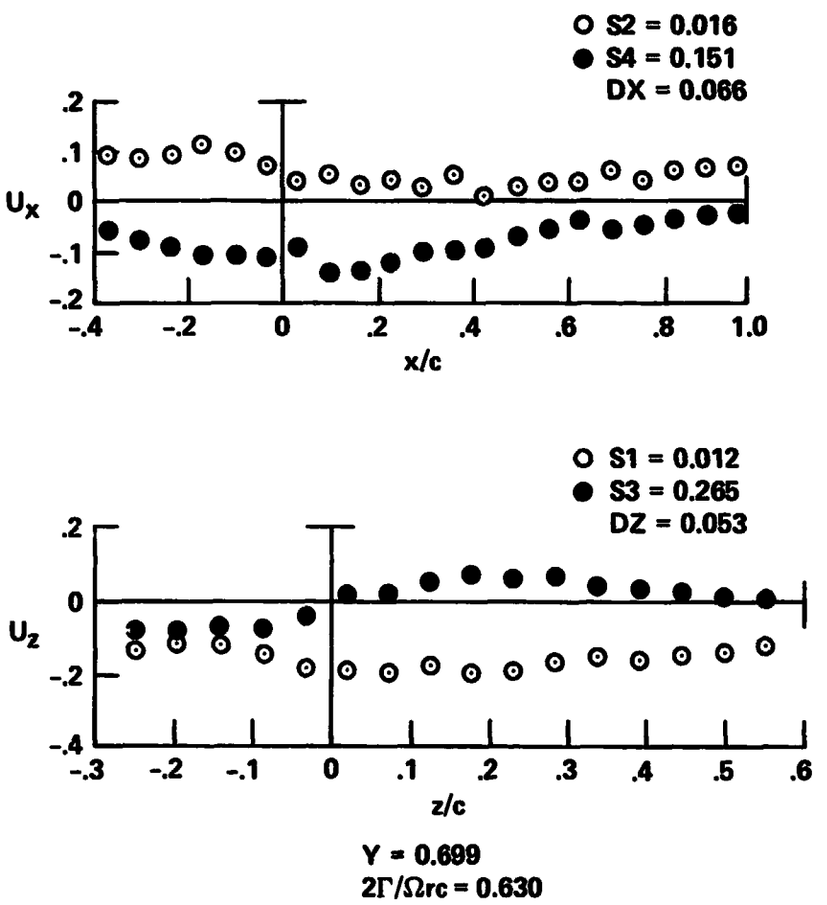

Figure 19.- Flow-field velocities about circulation contour at blade radial station 0.699R for rectangular blade tip.

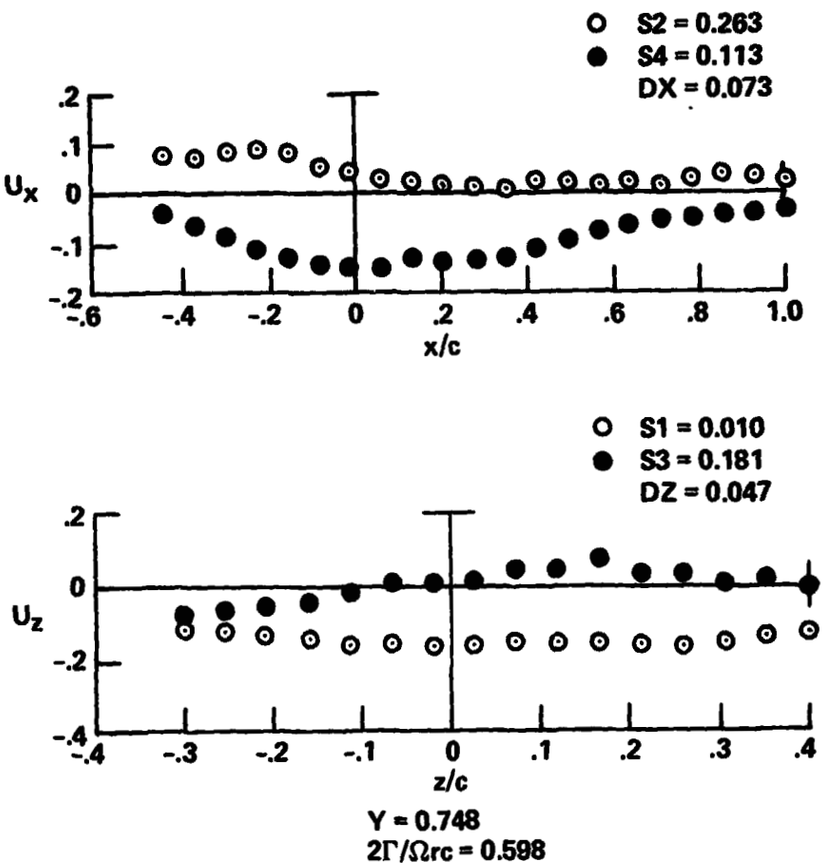

Figure 20.- Flow-field velocities about circulation contour at blade radial station 0.748R for rectangular blade tip.

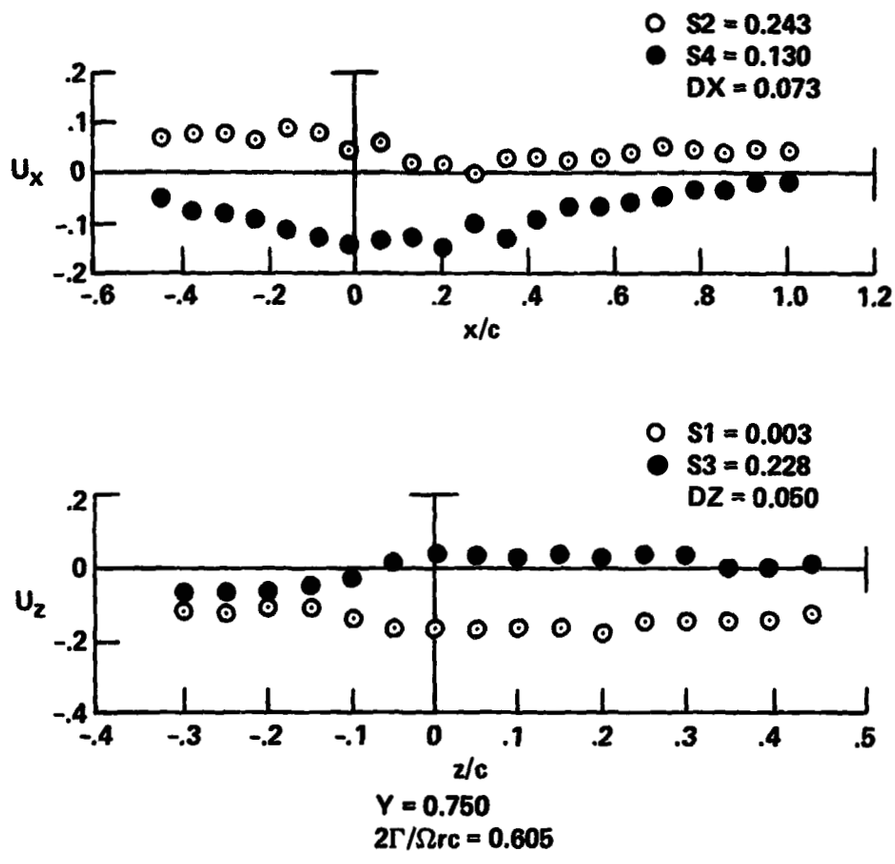

Figure 21.- Flow-field velocities about circulation contour at blade radial station 0.750R for rectangular blade tip.

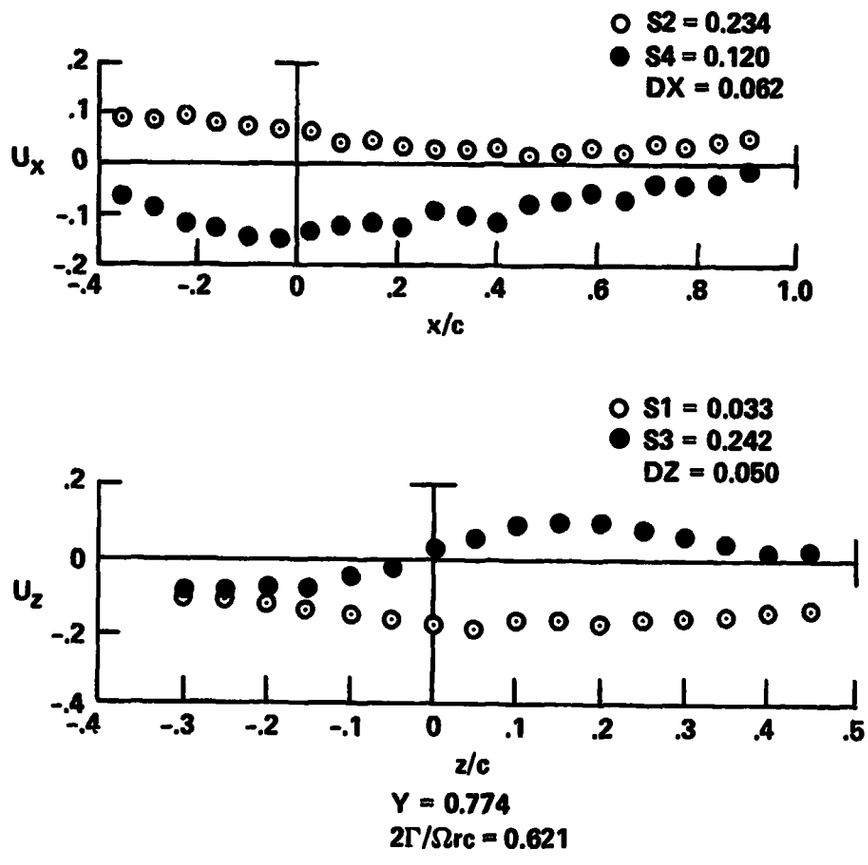

Figure 22.- Flow-field velocities about circulation contour at blade radial station 0.774R for rectangular blade tip.

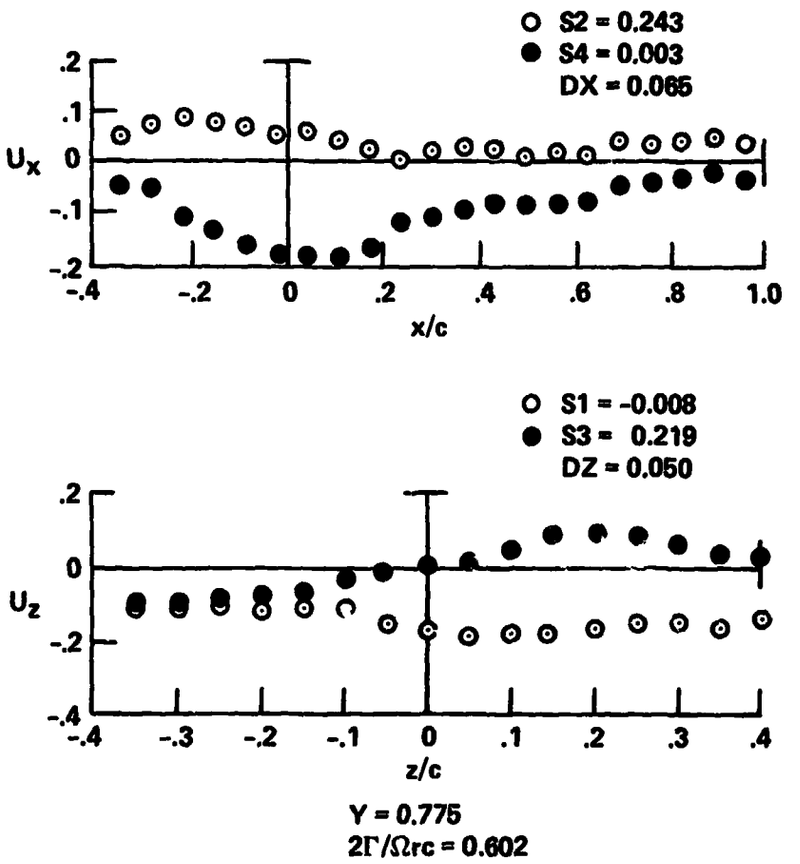

Figure 23.- Flow-field velocities about circulation contour at blade radial station 0.775R for rectangular blade tip.

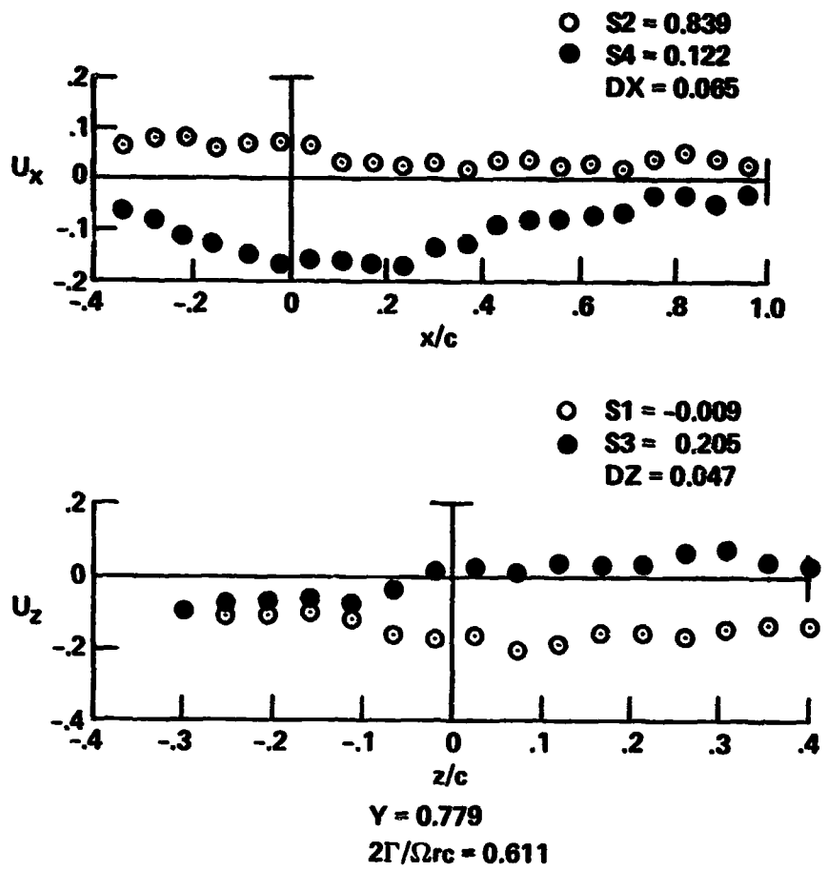

Figure 24.- Flow-field velocities about circulation contour at blade radial station 0.779R for rectangular blade tip.

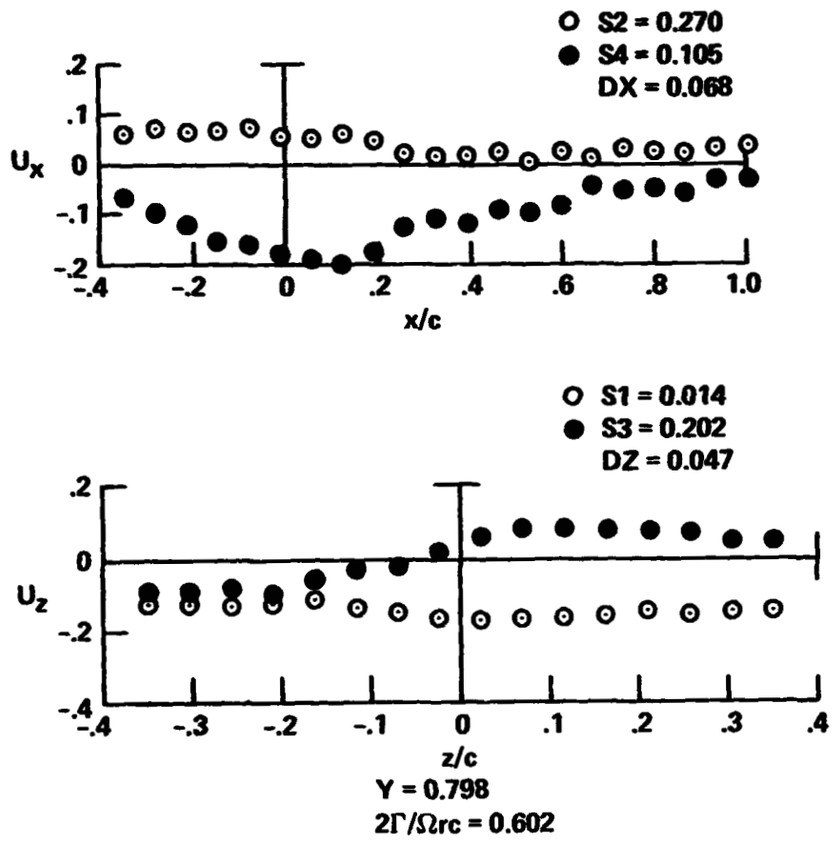

Figure 25.- Flow-field velocities about circulation contour at blade radial station 0.798R for rectangular blade tip.

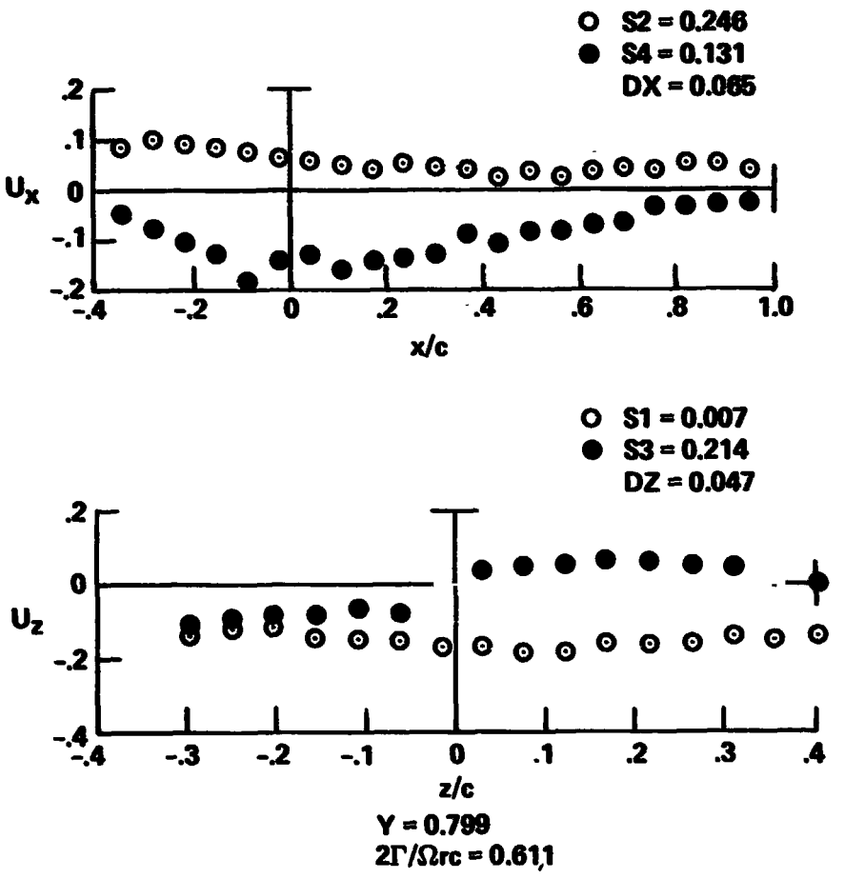

Figure 26.- Flow-field velocities about circulation contour at blade radial station 0.799R for rectangular blade tip.

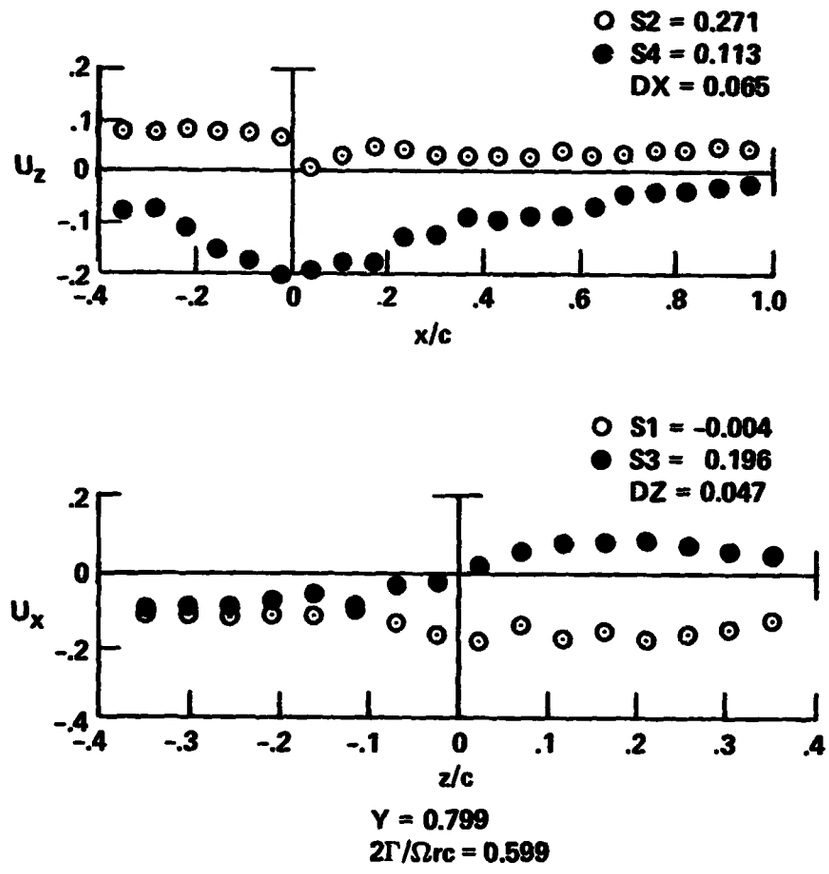

Figure 27.- Flow-field velocities about circulation contour at blade radial station 0.799R for rectangular blade tip.

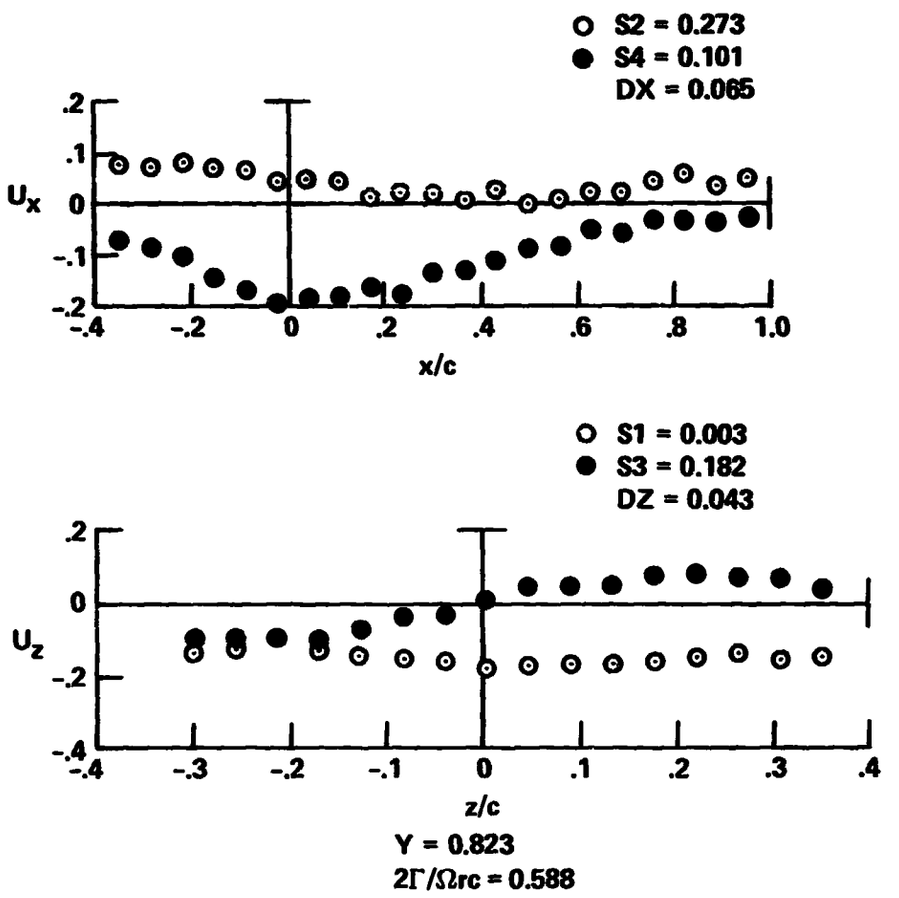

Figure 28.- Flow-field velocities about circulation contour at blade radial station 0.823R for rectangular blade tip.

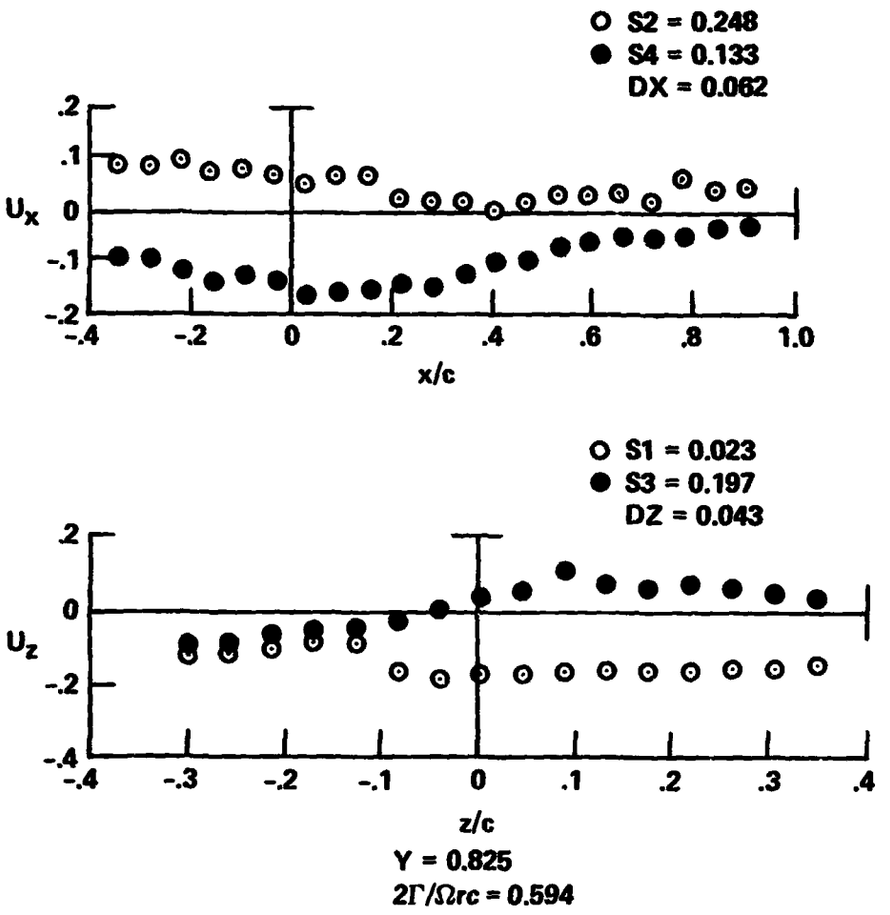

Figure 29.- Flow-field velocities about circulation contour at blade radial station 0.825R for rectangular blade tip.

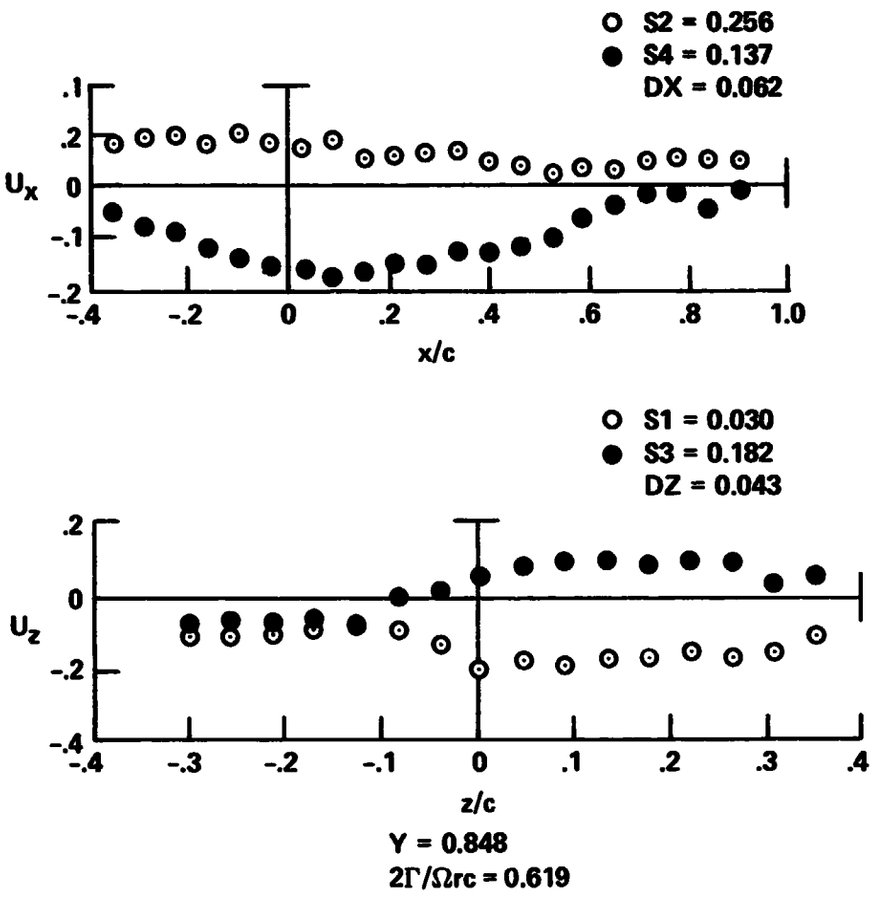

Figure 30.- Flow-field velocities about circulation contour at blade radial station 0.848R for rectangular blade tip.

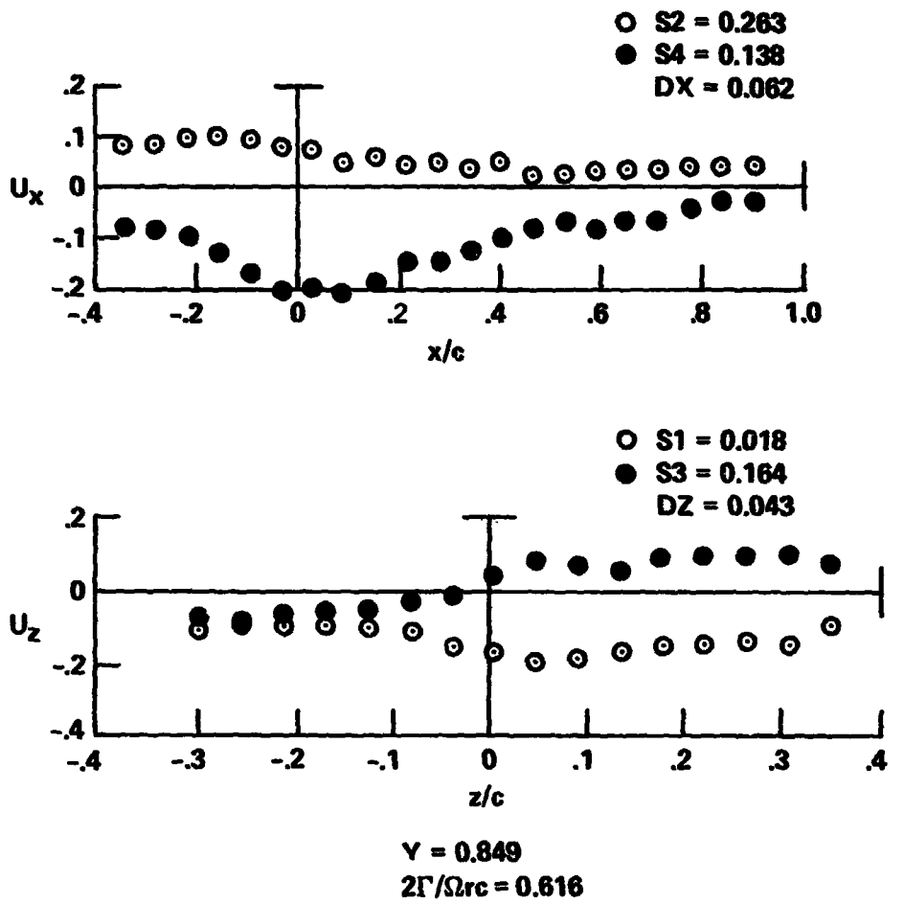

Figure 31.- Flow-field velocities about circulation contour at blade radial station 0.849R for rectangular blade tip.

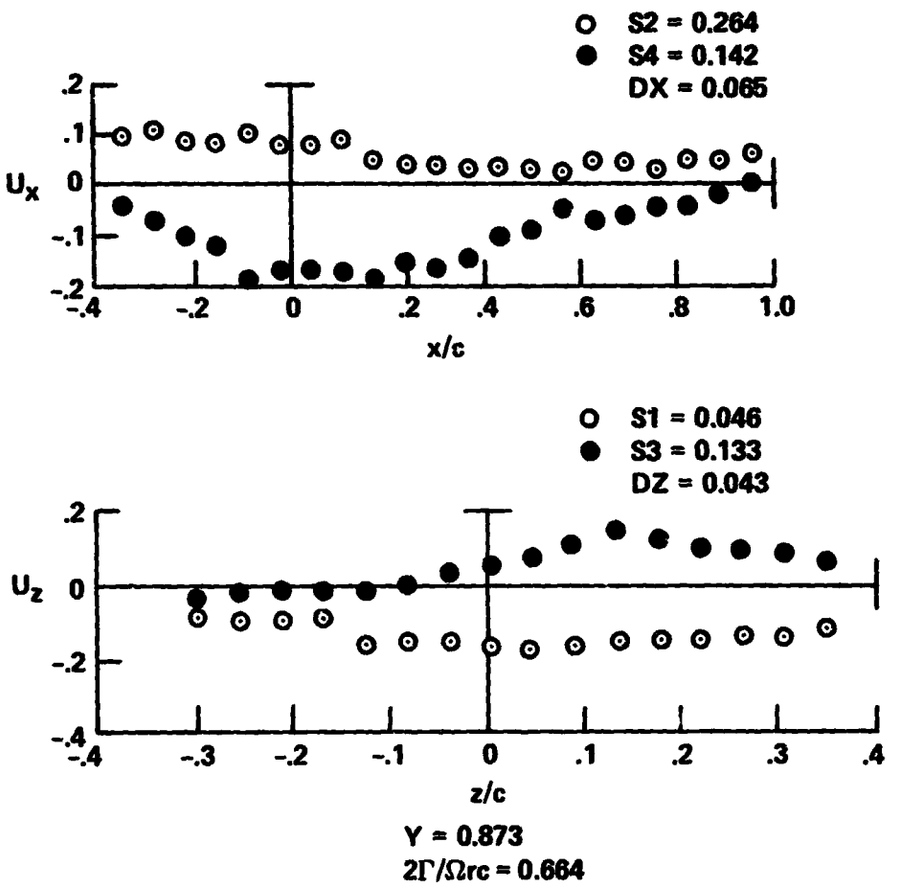

Figure 32.- Flow-field velocities about circulation contour at blade radial station 0.873R for rectangular blade tip.

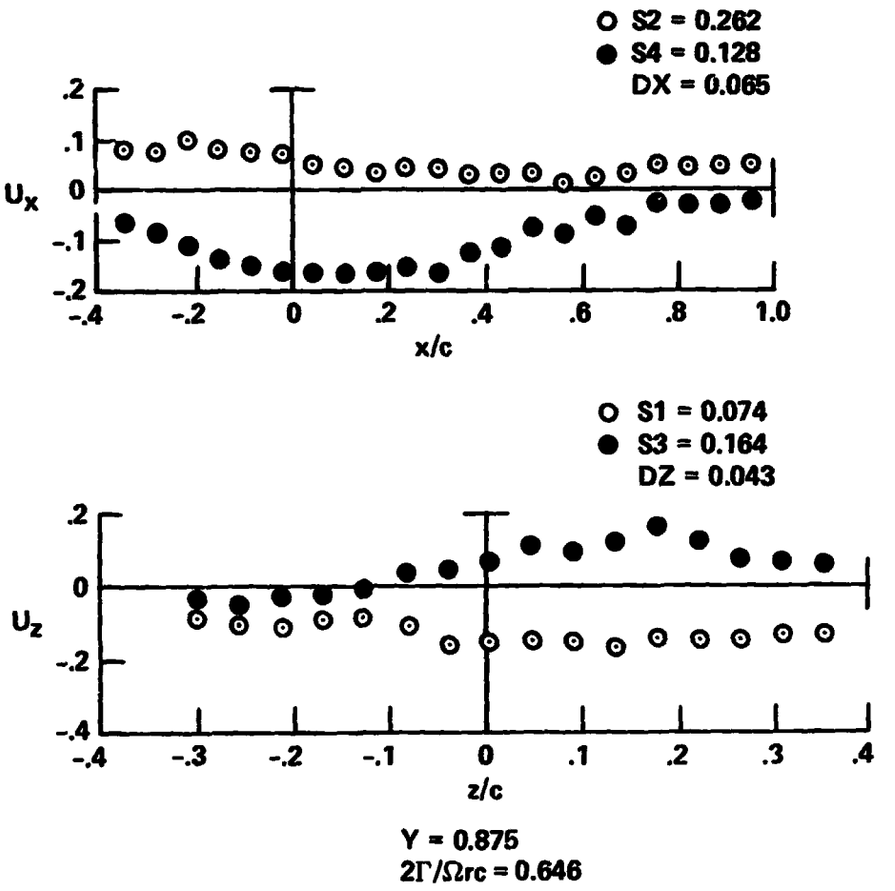

Figure 33.- Flow-field velocities about circulation contour at blade radial station 0.875R for rectangular blade tip.

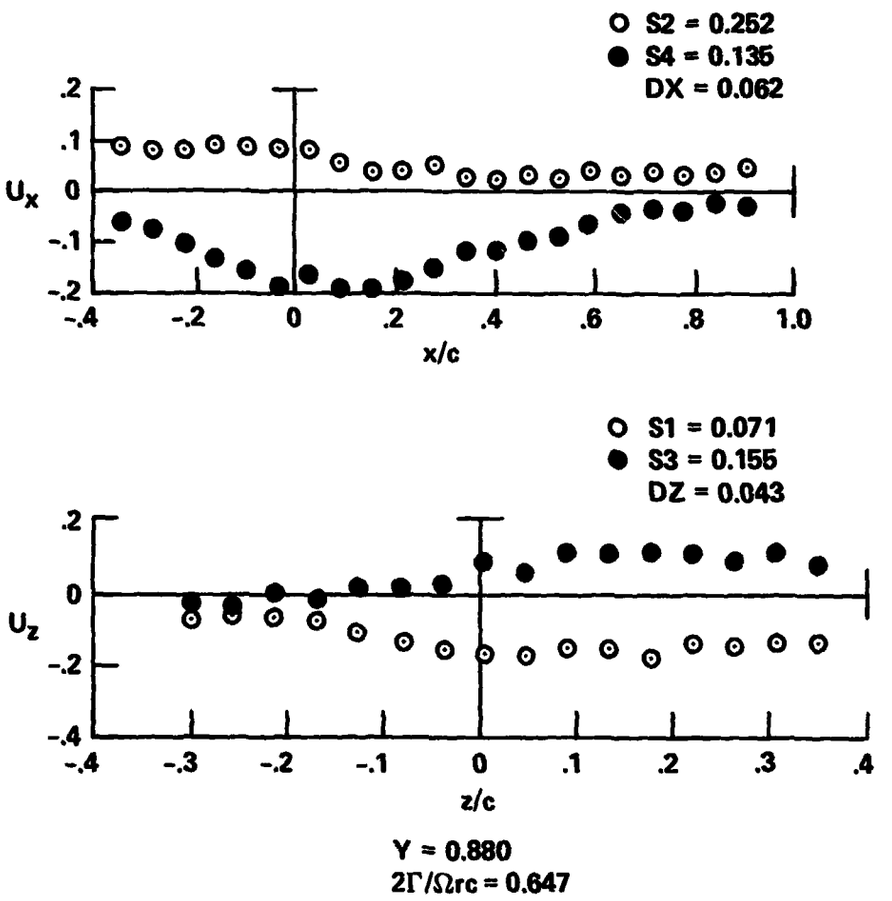

Figure 34.- Flow-field velocities about circulation contour at blade radial station 0.880R for rectangular blade tip.

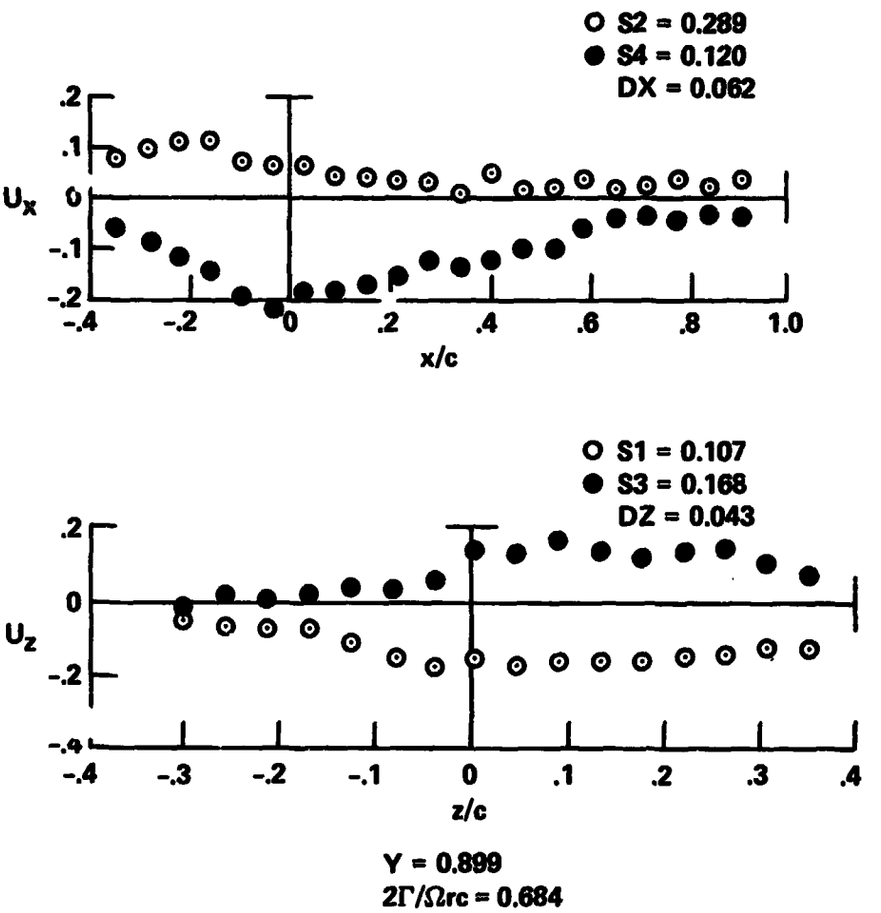

Figure 35.- Flow-field velocities about circulation contour at blade radial station 0.899R for rectangular blade tip.

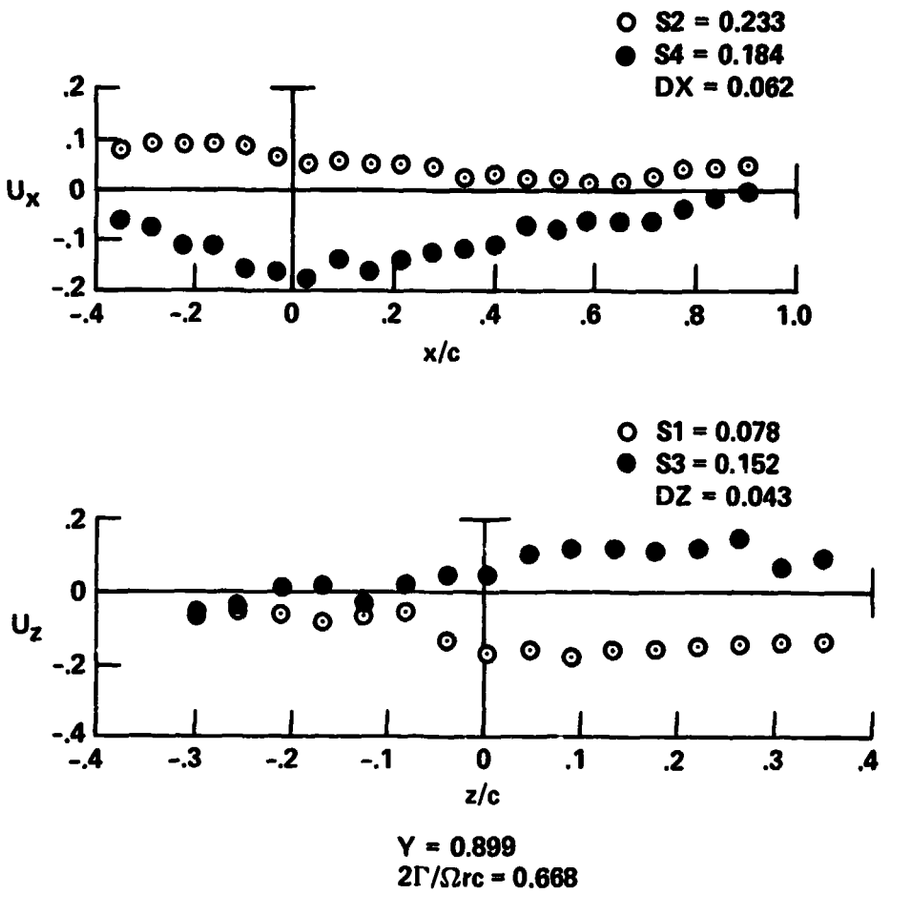

Figure 36.- Flow-field velocities about circulation contour at blade radial station 0.899R for rectangular blade tip.

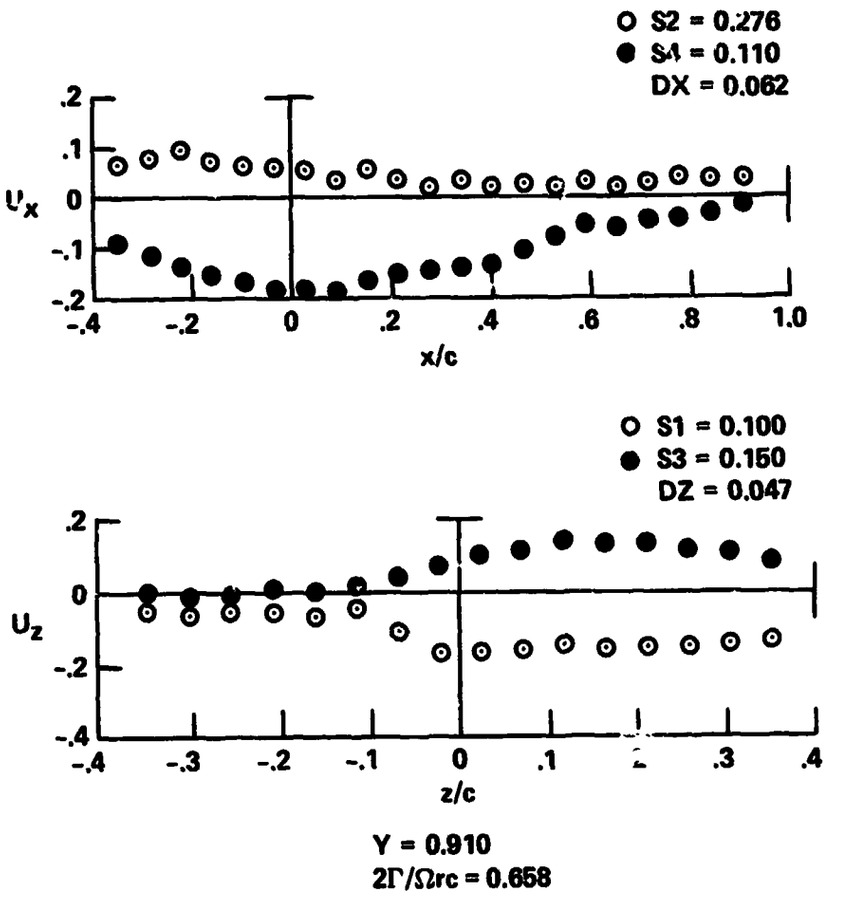

Figure 37.- Flow-fieid velocities about circulation contour at blade radial station 0.910R for rectangular blade tip.

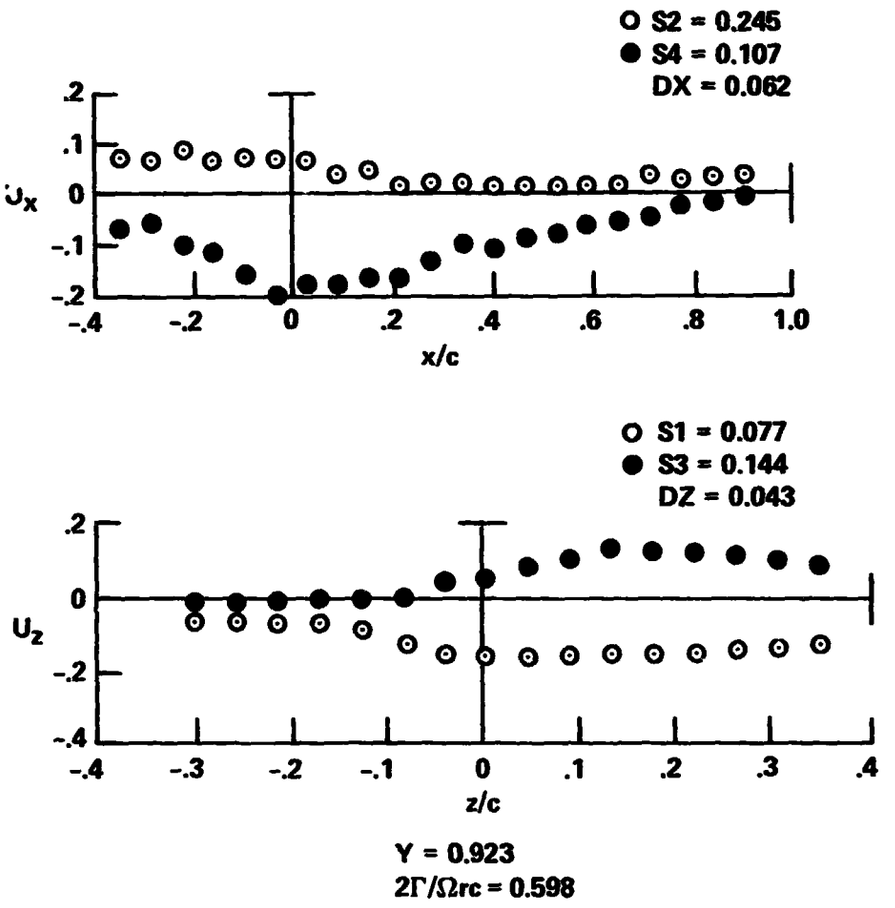

Figure 38.- Flow-field velocities about circulation contour at blade radial station 0.923R for rectangular blade tip.

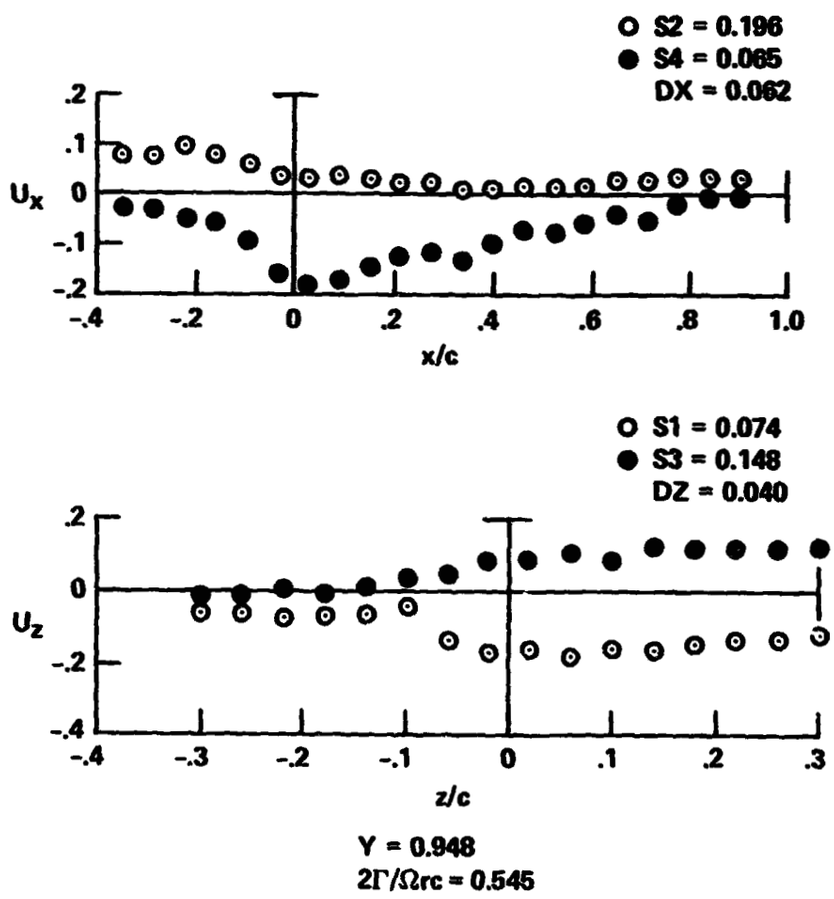

Figure 39.- Flow-field velocities about circulation contour at blade radial station 0.948R for rectangular blade tip.

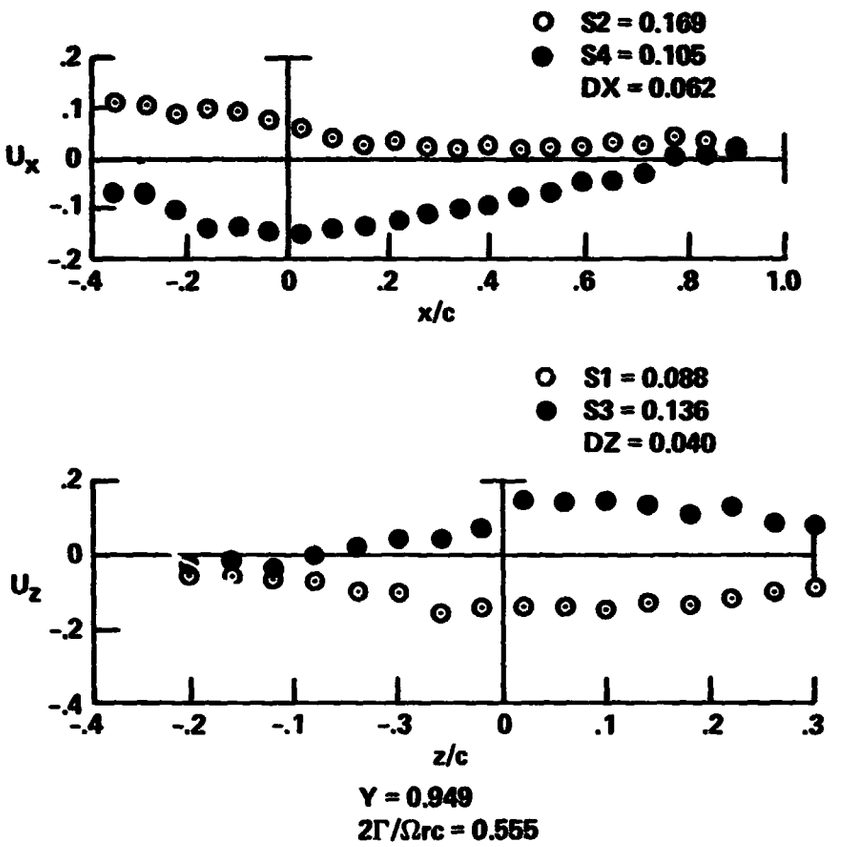

Figure 40.- Flow-field velocities about circulation contour at blade radial station 0.949R for rectangular blade tip.

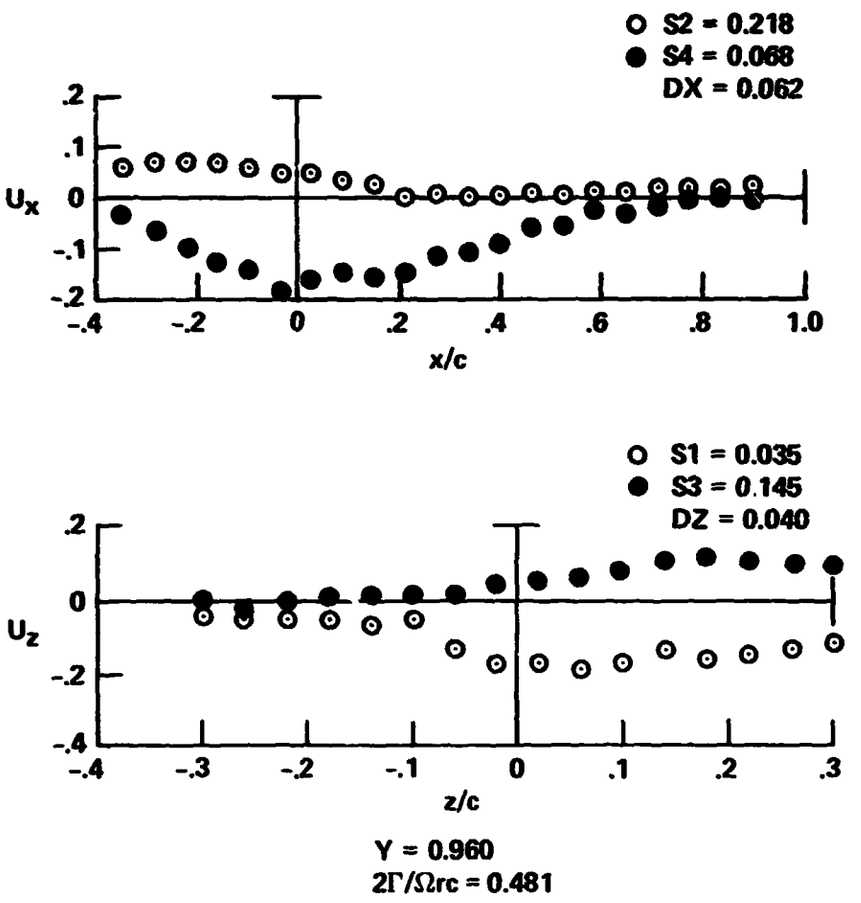

Figure 41.- Flow-field velocities about circulation contour at blade radial station 0.960R for rectangular blade tip.

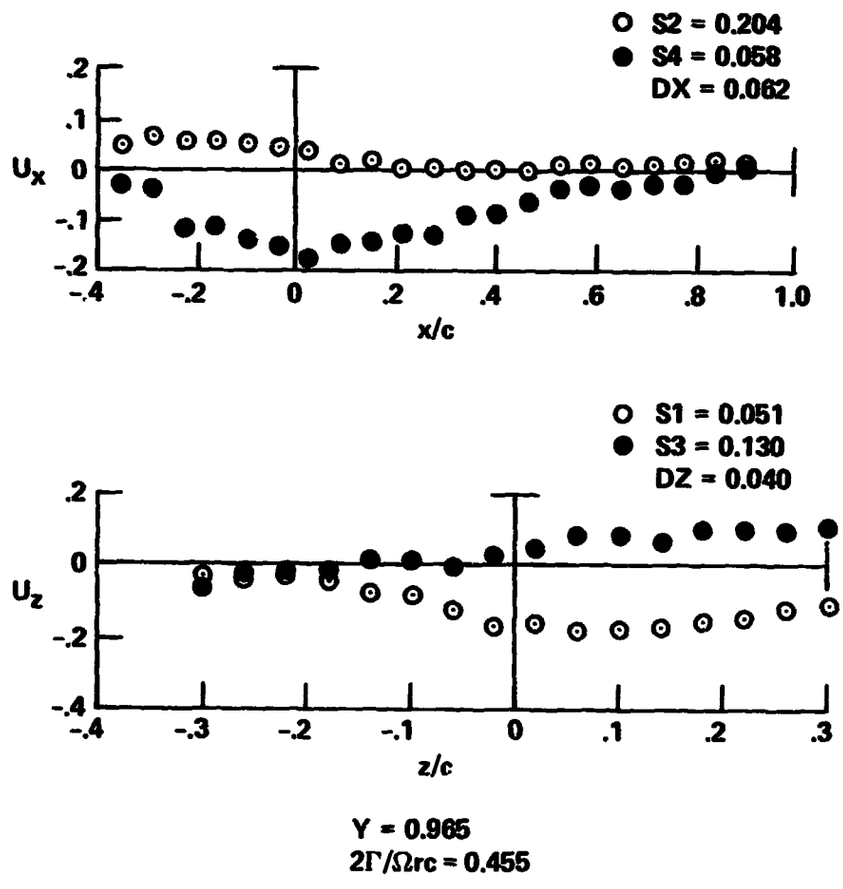

Figure 42.- Flow-field velocities about circulation contour at blade radial station 0.965R for rectangular blade tip.

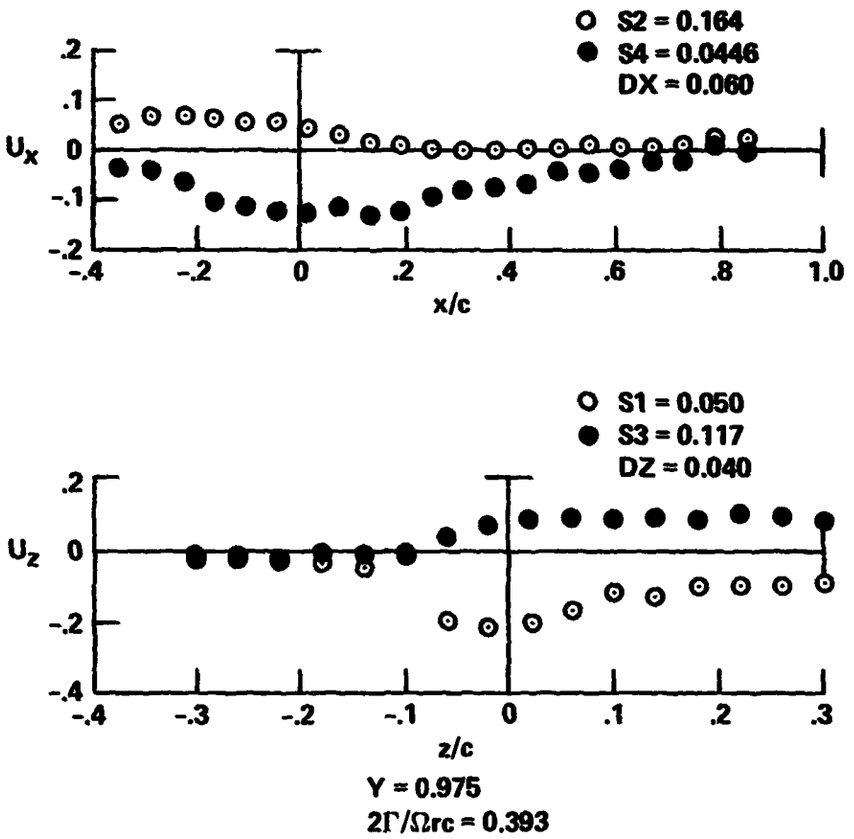

Figure 43.- Flow-field velocities about circulation contour at blade radial station 0.975R for rectangular blade tip.

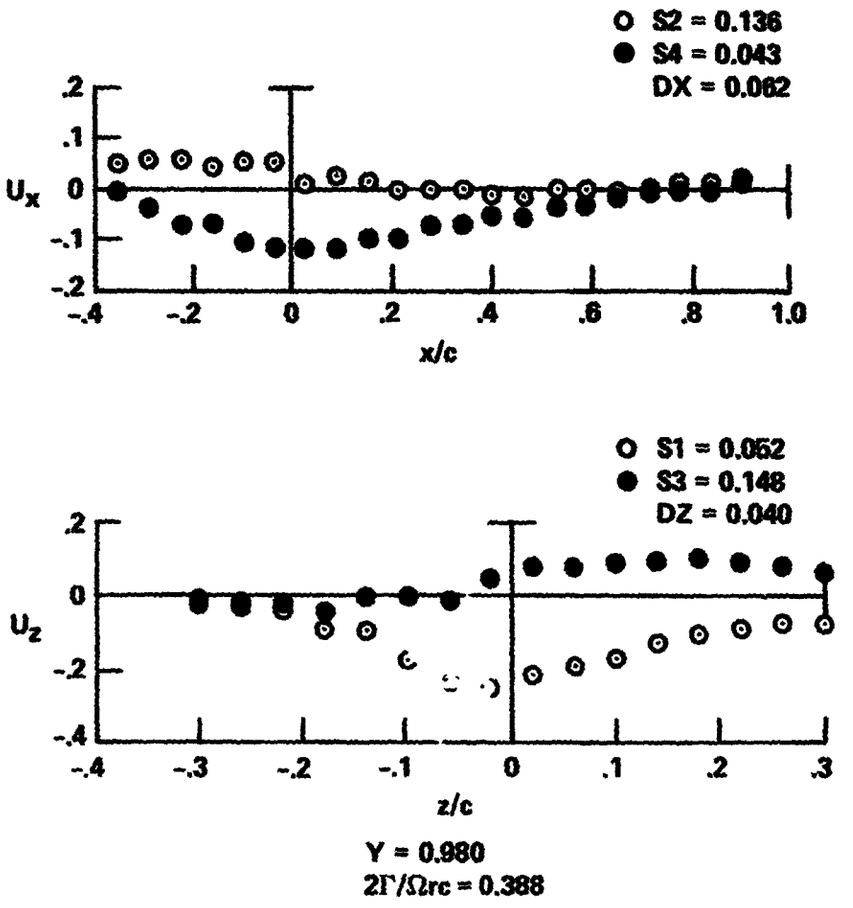

Figure 44.- Flow-field velocities about circulation contour at blade radial station 0.980R for rectangular blade tip.

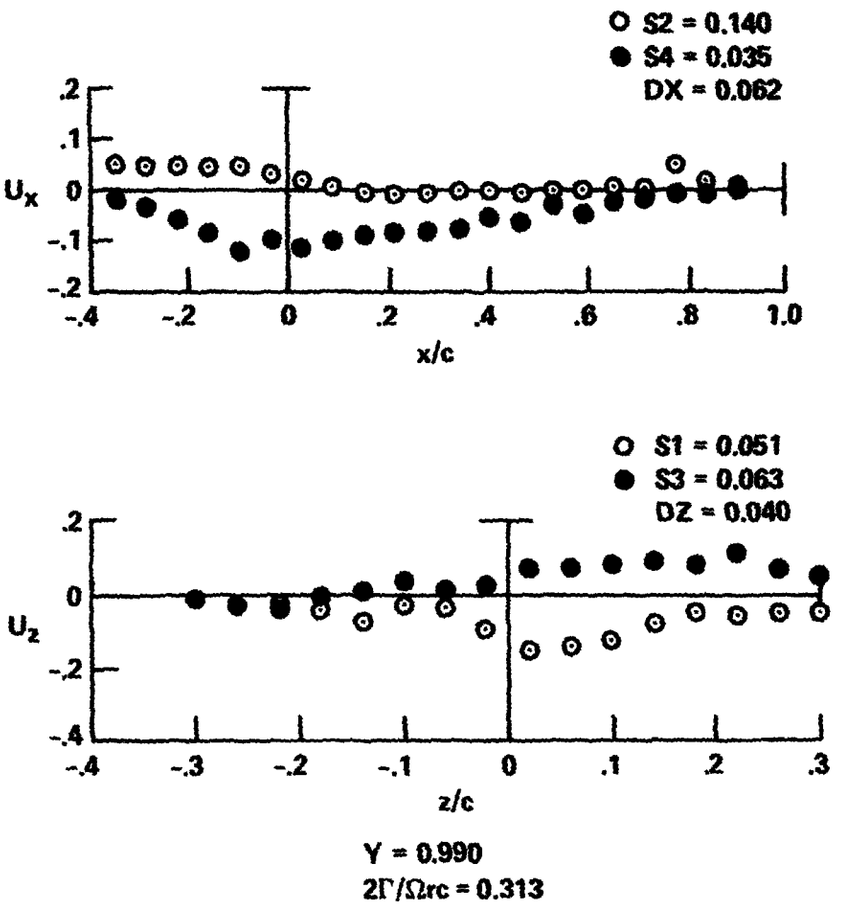

Figure 45.- Flow-field velocities about circulation contour at blade radial station 0.990R for rectangular blade tip.

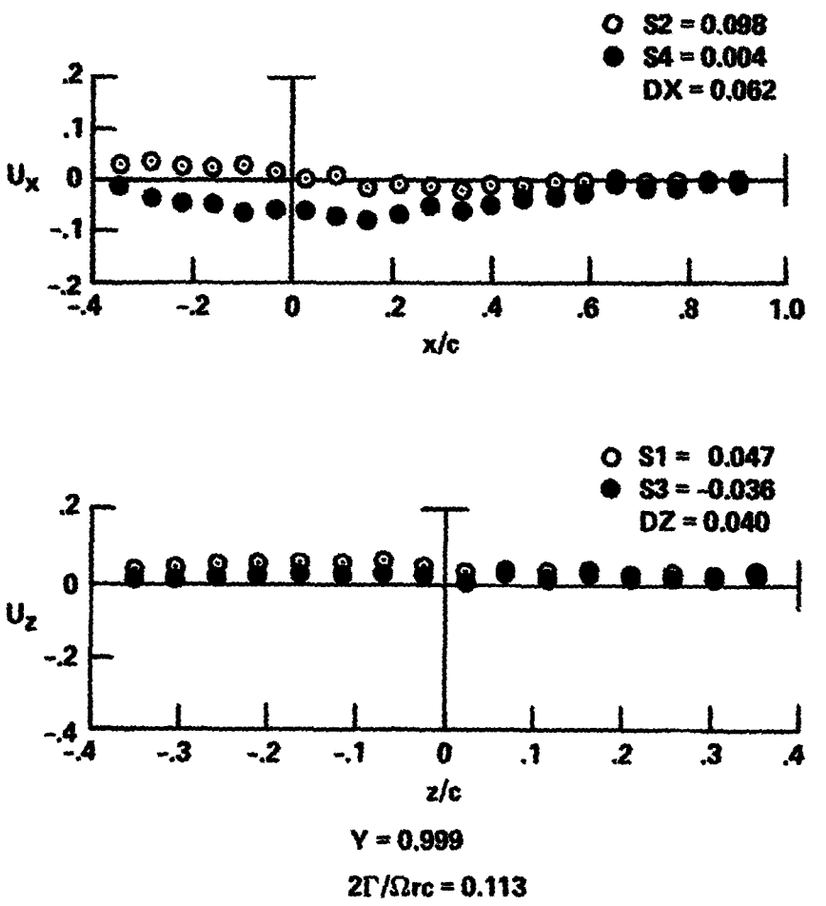

Figure 46.- Flow-field velocities about circulation contour at blade radial station 0.999R for rectangular blade tip.

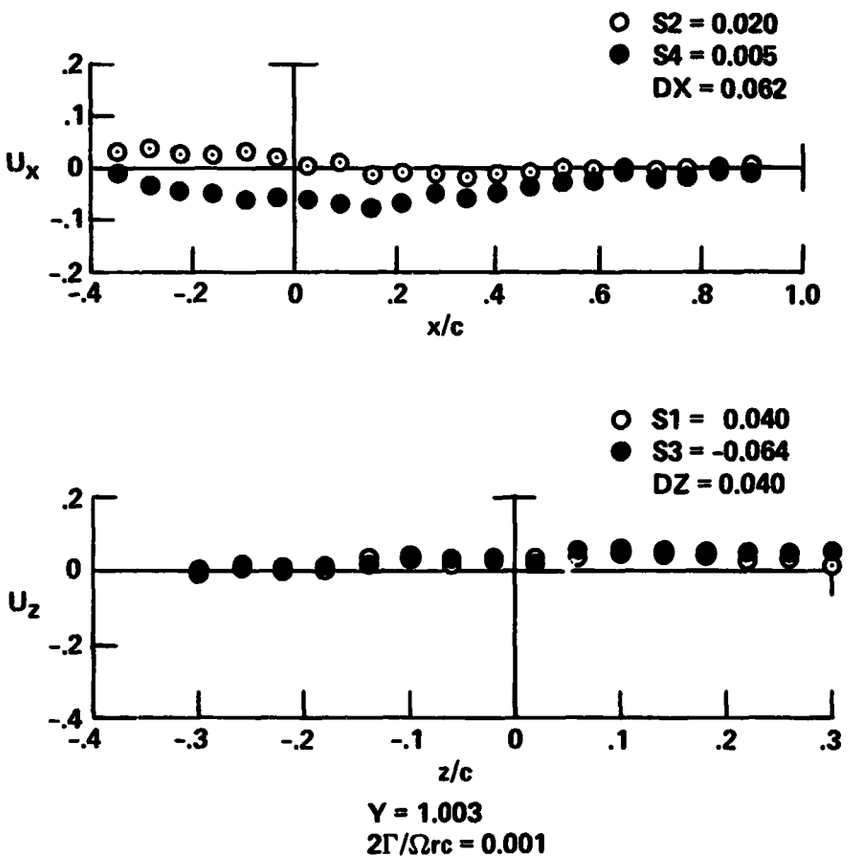

Figure 47.- Flow-field velocities about circulation contour at blade radial station 1.003R for rectangular blade tip.

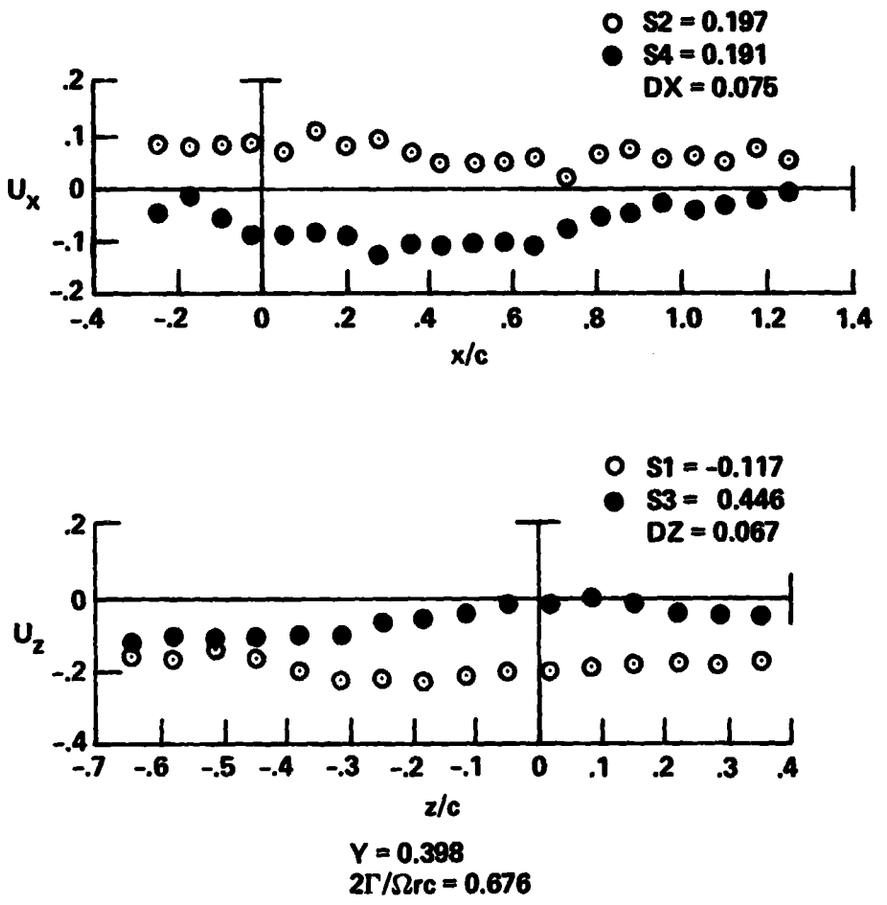

Figure 48.- Flow-field velocities about circulation contour at blade radial station 0.398R for ogee blade tip.

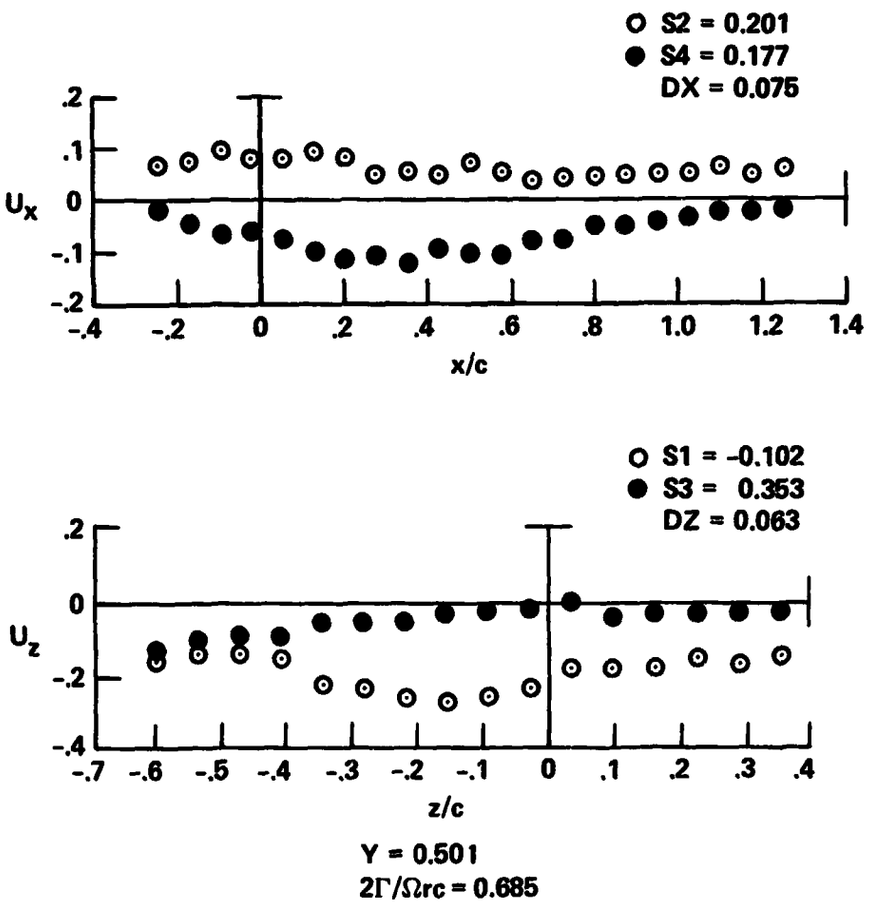

Figure 49.- Flow-field velocities about circulation contour at blade radial station 0.501R for ogee blade tip.

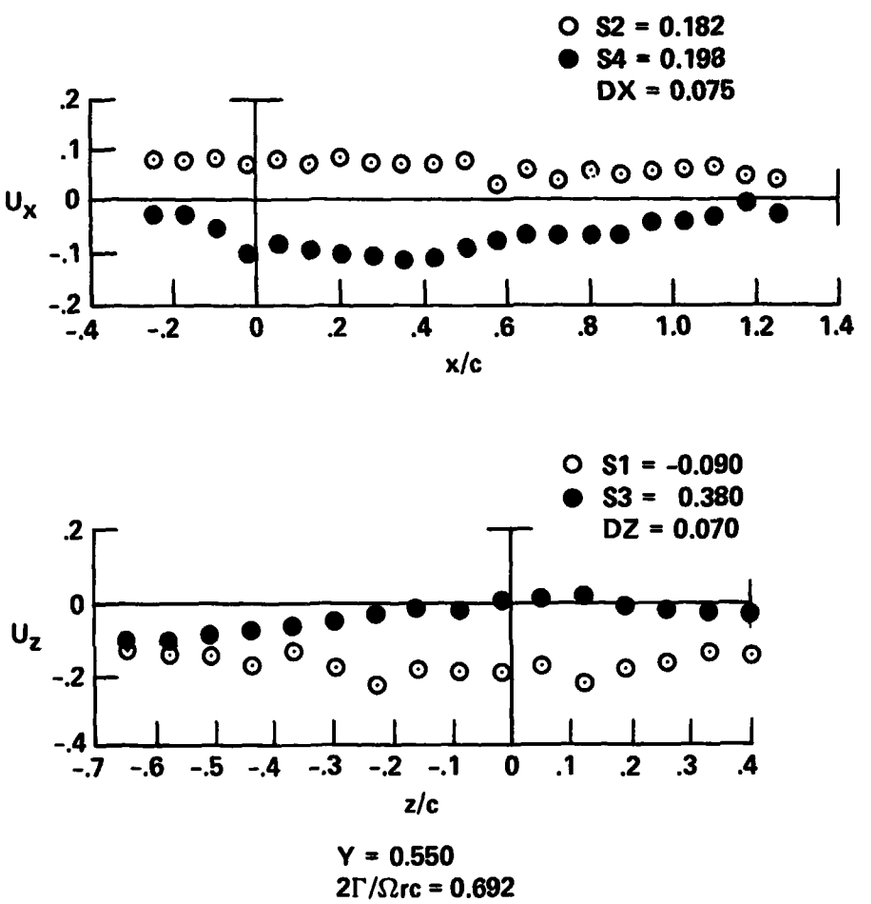

Figure 50.- Flow-field velocities about circulation contour at blade radial station 0.550R for ogee blade tip.

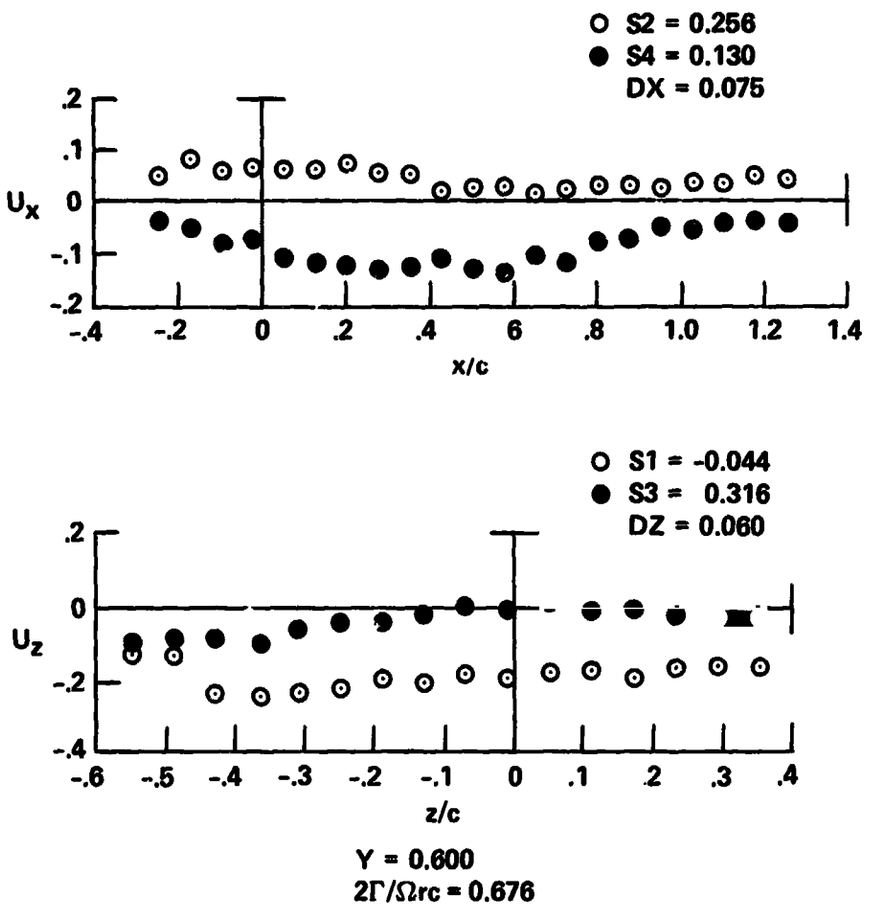

Figure 51.- Flow-field velocities about circulation contour at blade radial station 0.600R for ogee blade tip.

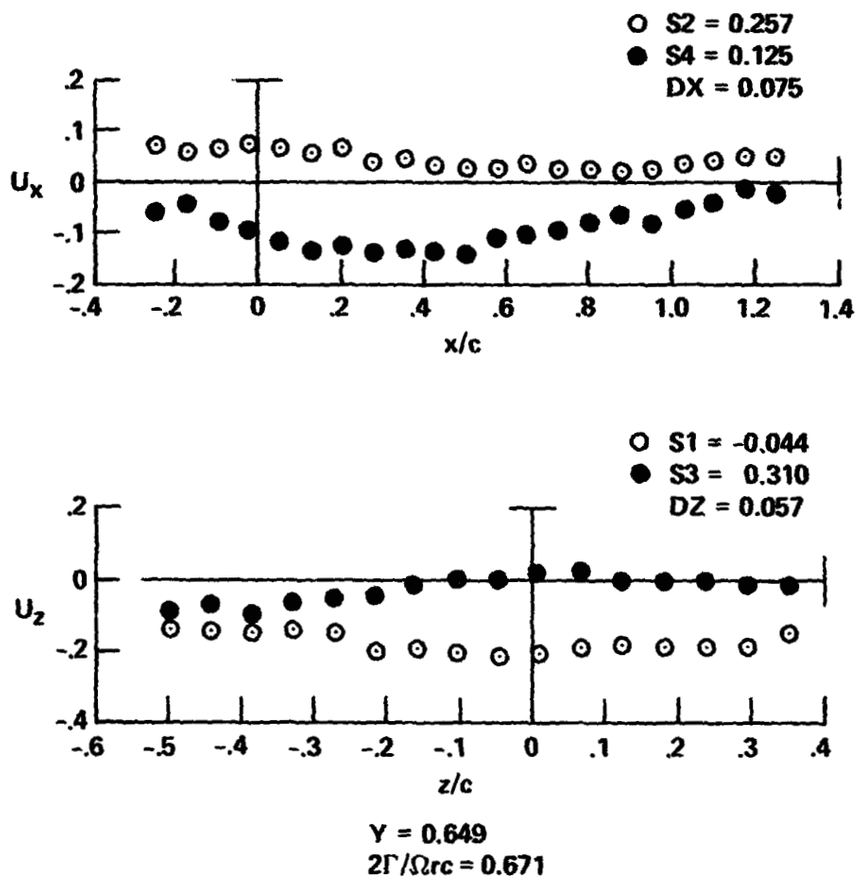

Figure 52.- Flow-field velocities about circulation contour at blade radial station 0.649R for ogee blade tip.

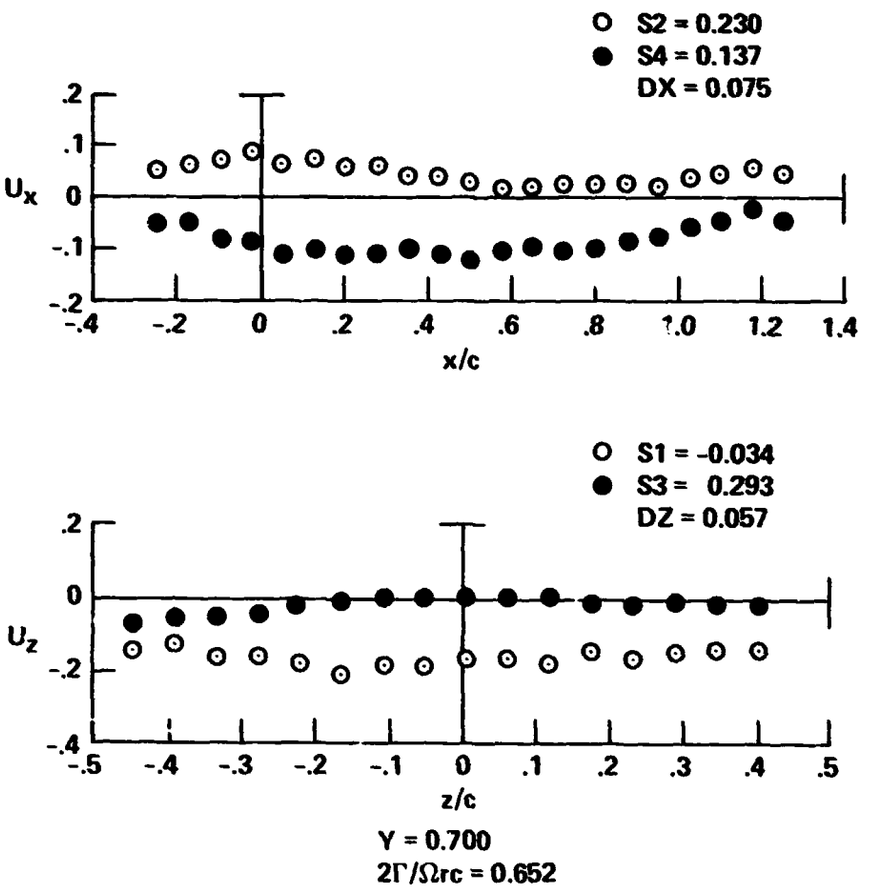

Figure 53.- Flow-field velocities about circulation contour at blade radial station 0.700R for ogee blade tip.

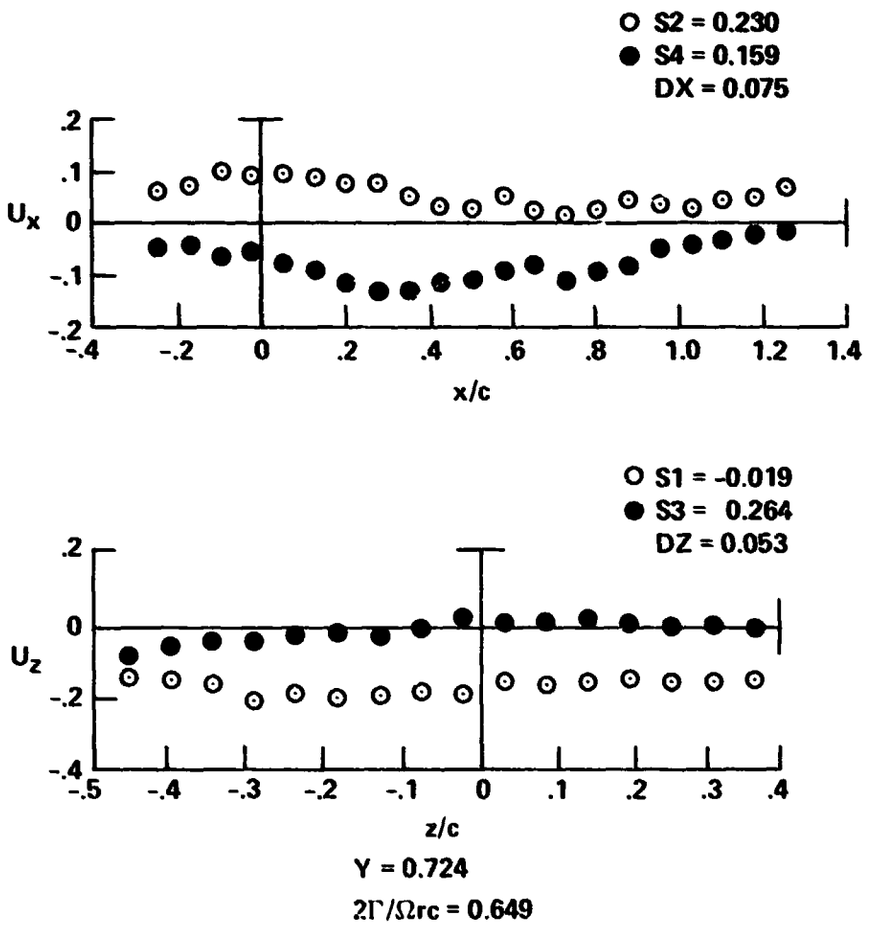

Figure 54.- Flow-field velocities about circulation contour at blade radial station 0.724R for ogee blade tip.

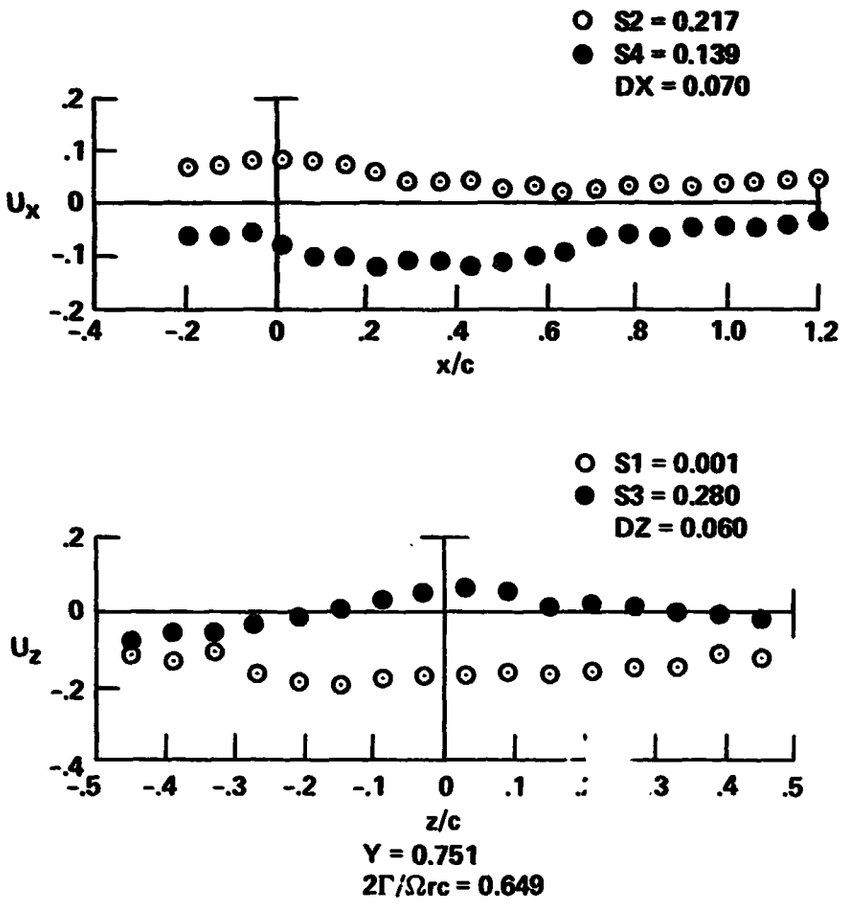

Figure 55.- Flow-field velocities about circulation contour at blade radial station 0.751R for ogee blade tip.

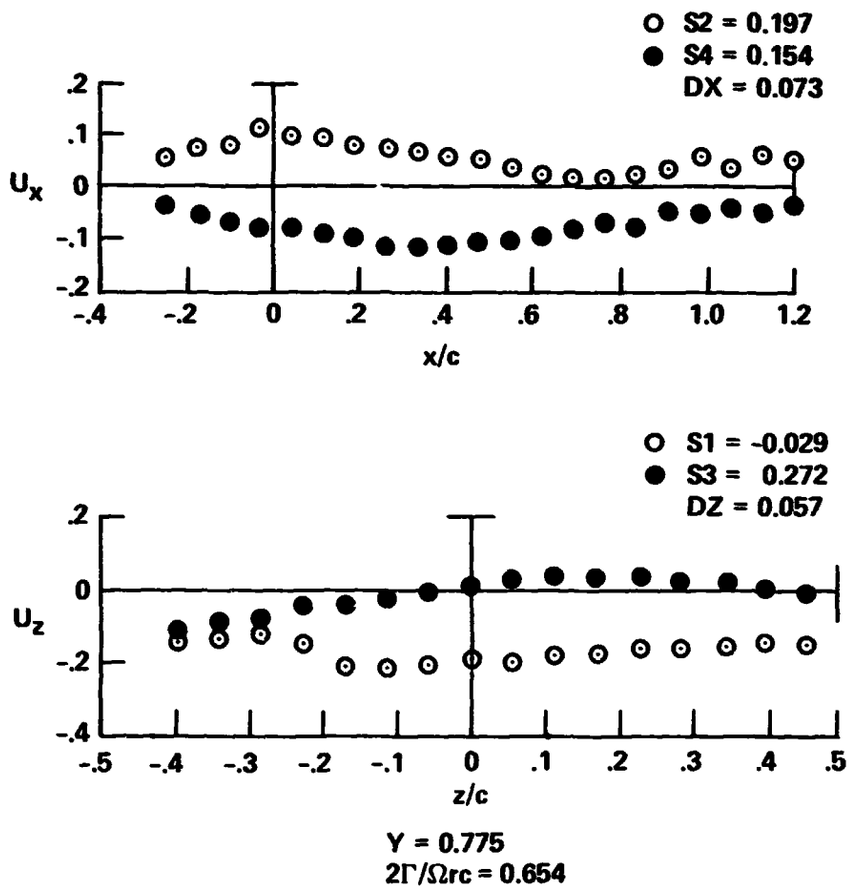

Figure 56.- Flow-field velocities about circulation contour at blade radial station 0.775R for ogee blade tip.

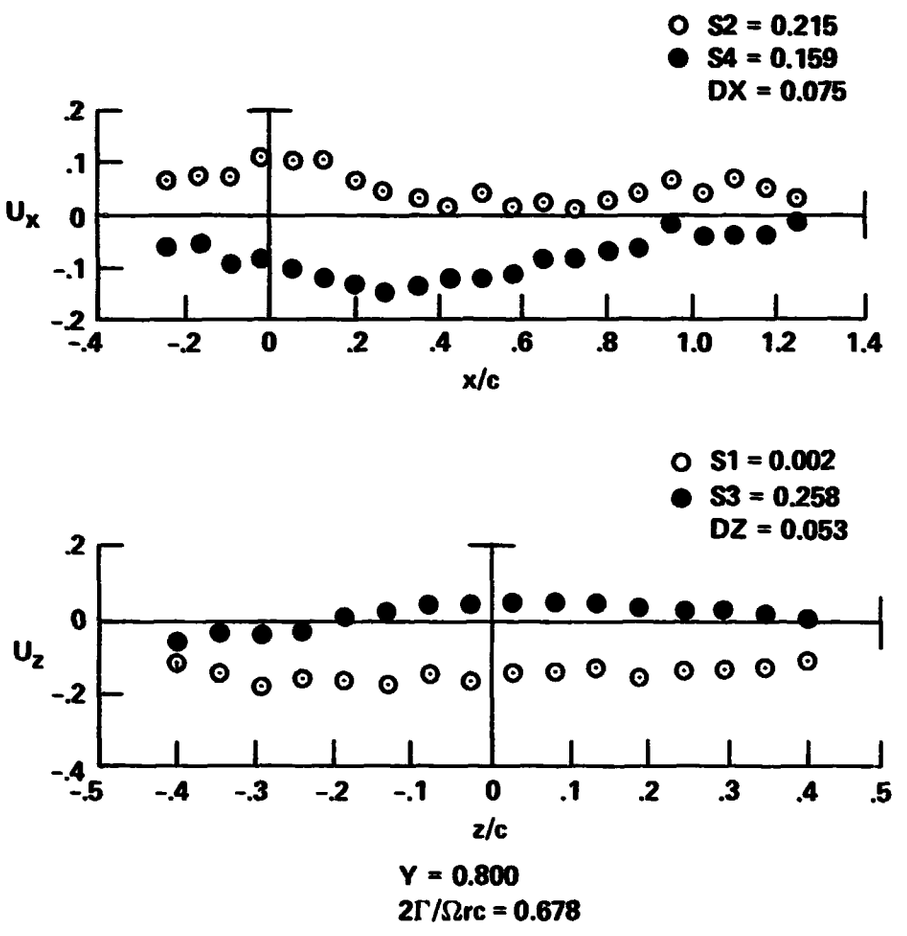

Figure 57.- Flow-field velocities about circulation contour at blade radial station 0.800R for ogee blade tip.

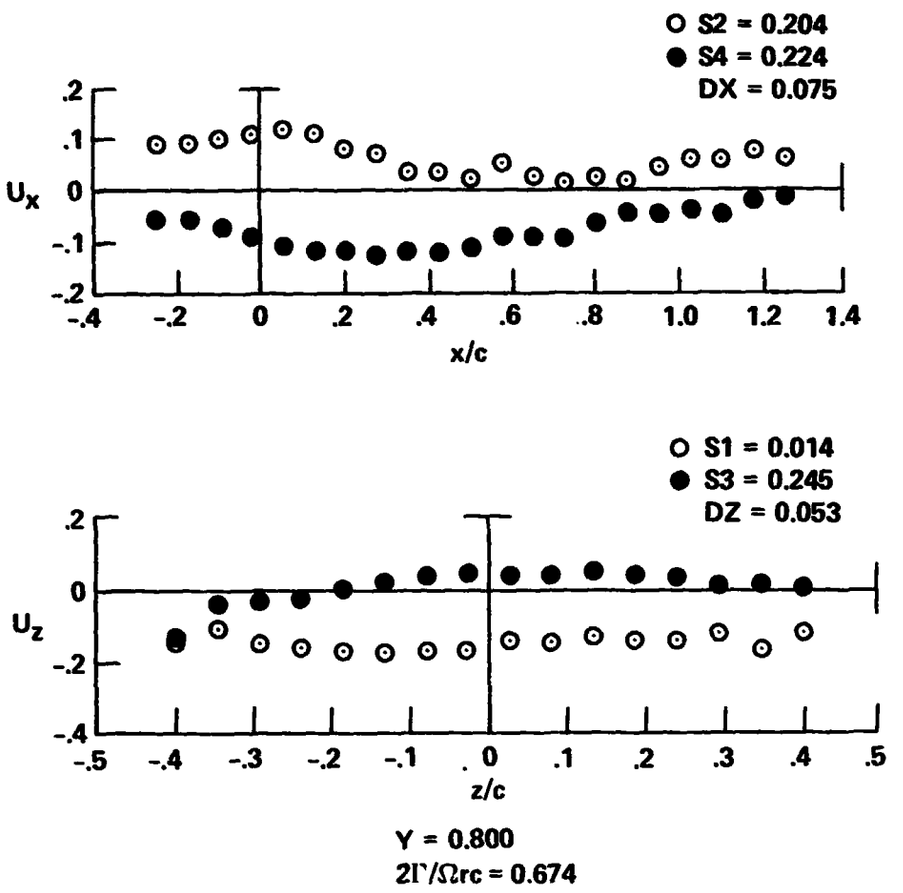

Figure 58.- Flow-field velocities about circulation contour at blade radial station 0.800R for ogee blade tip.

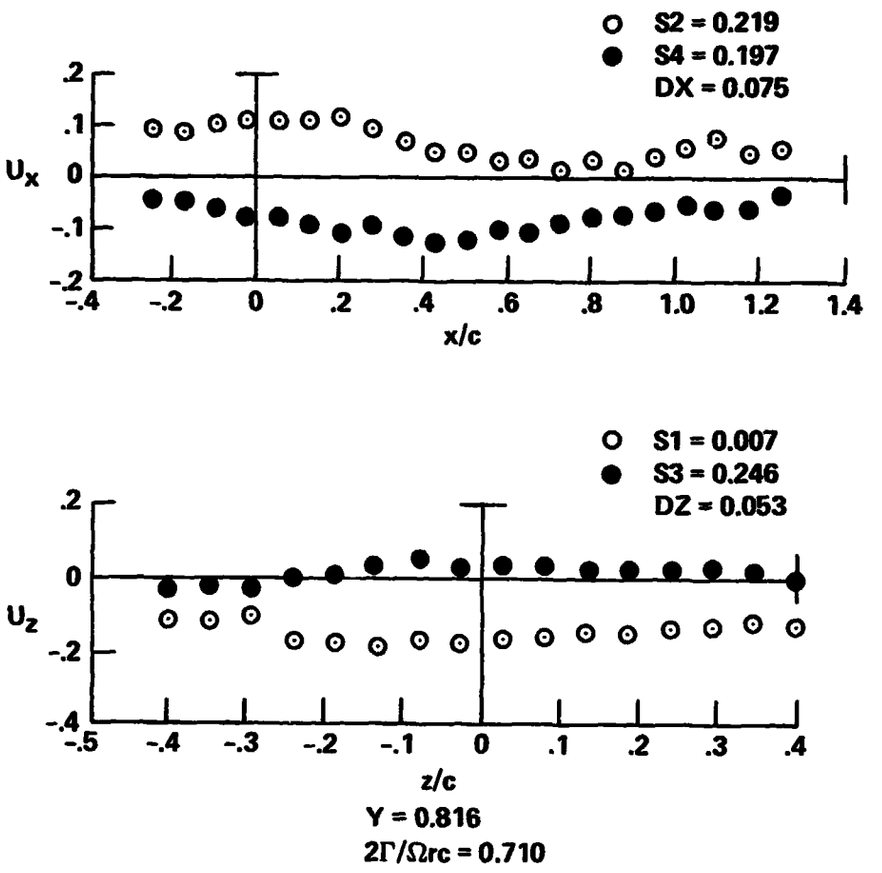

Figure 59.- Flow-field velocities about circulation contour at blade radial station 0.816R for ogee blade tip.

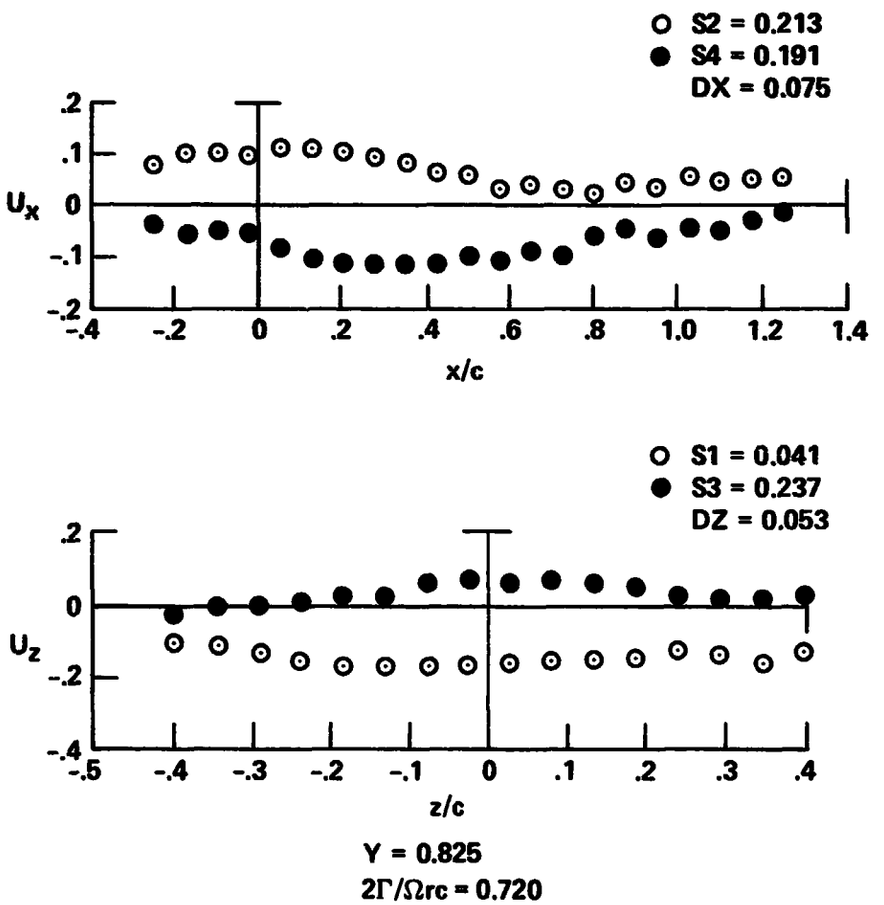

Figure 60.- Flow-field velocities about circulation contour at blade radial station 0.825R for ogee blade tip.

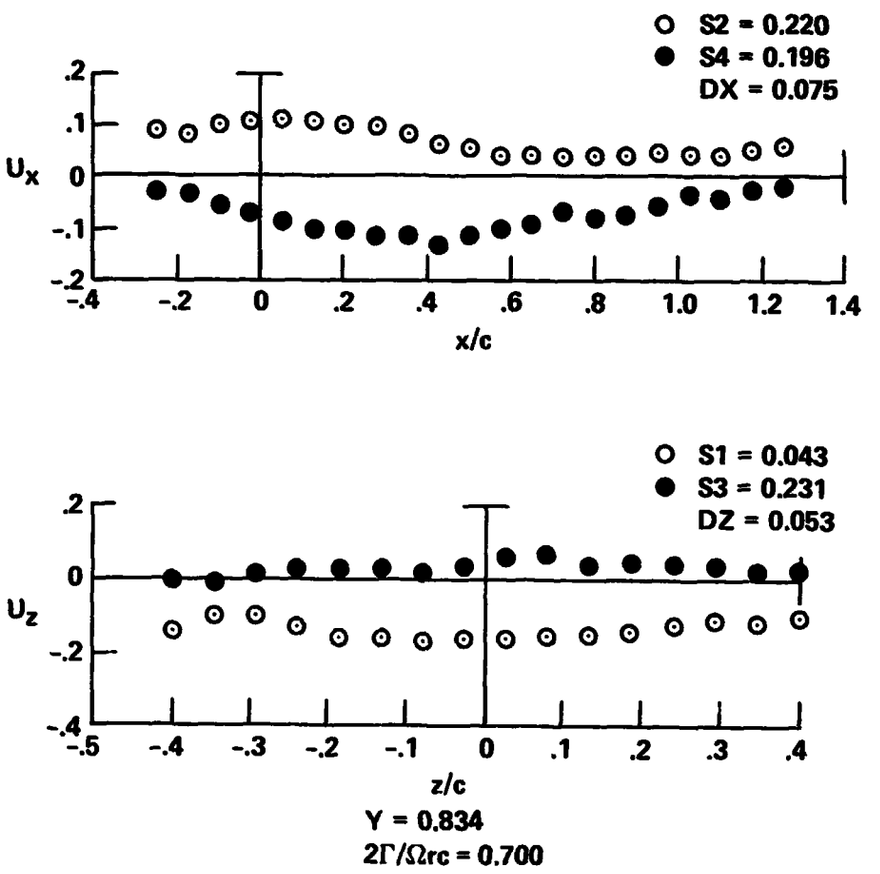

Figure 61.- Flow-field velocities about circulation contour at blade radial station 0.834R for ogee blade tip.

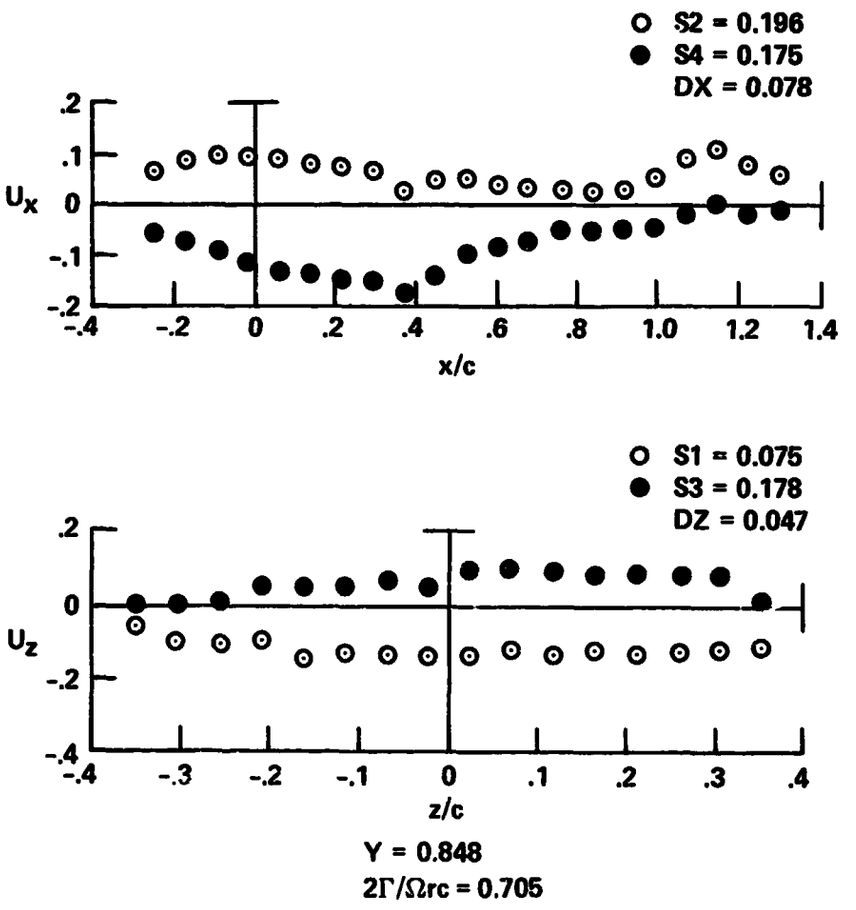

Figure 62.- Flow-field velocities about circulation contour at blade radial station 0.848R for ogee blade tip.

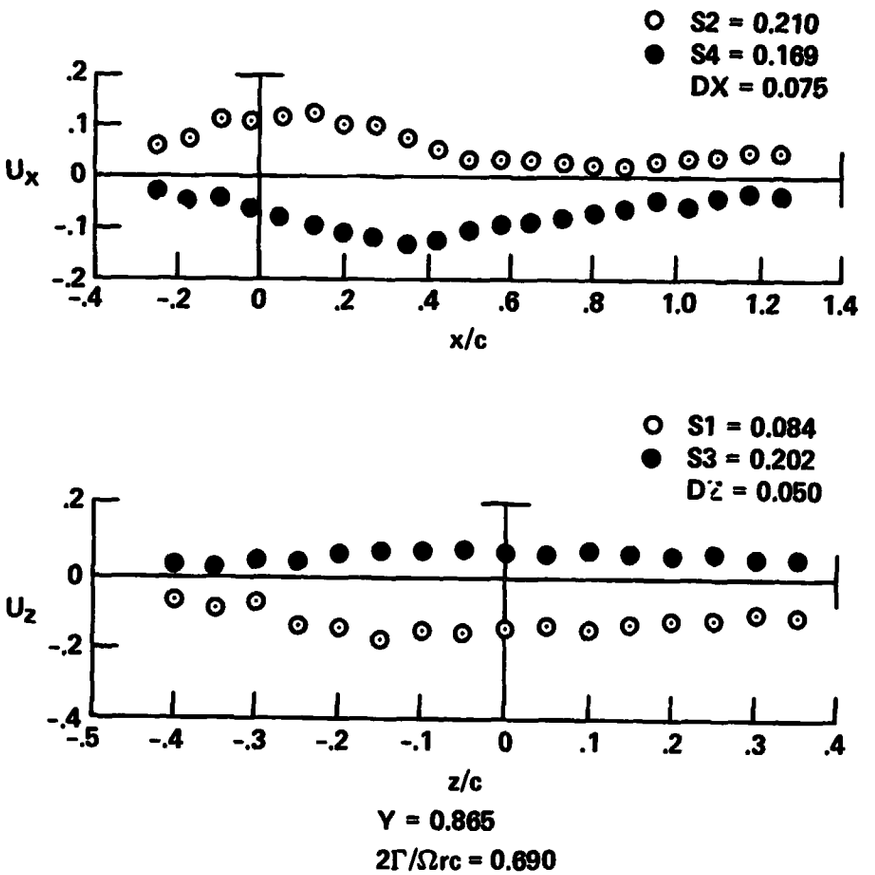

Figure 63.- Flow-field velocities about circulation contour at blade radial station 0.865R for ogee blade tip.

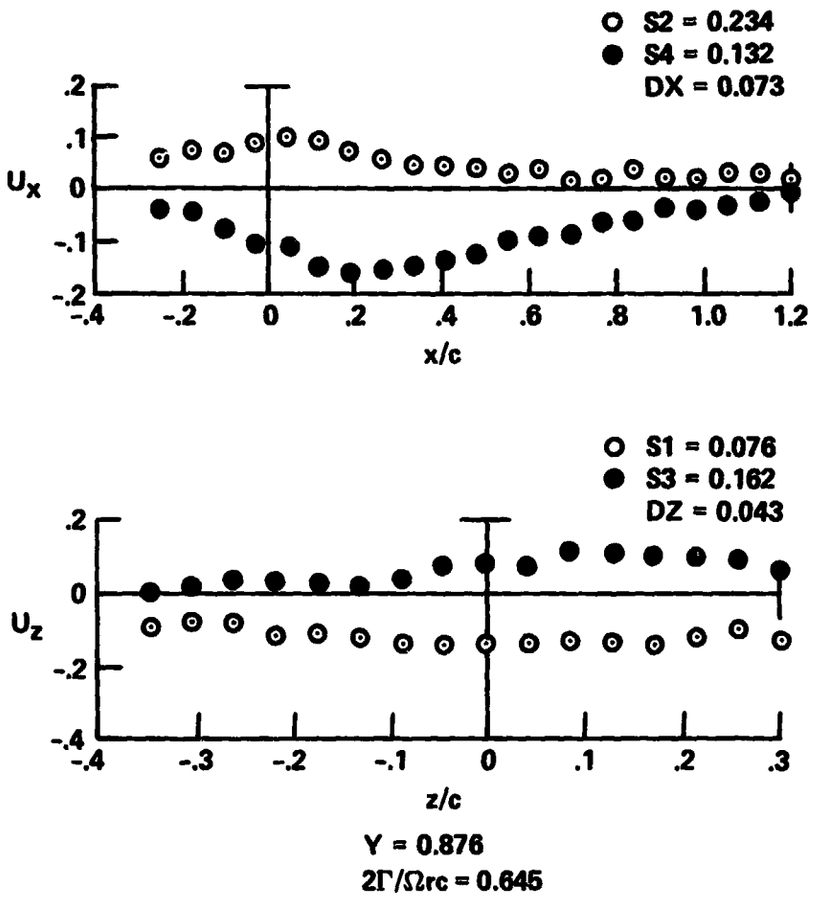

Figure 64.- Flow-field velocities about circulation contour at blade radial station 0.876R for ogee blade tip.

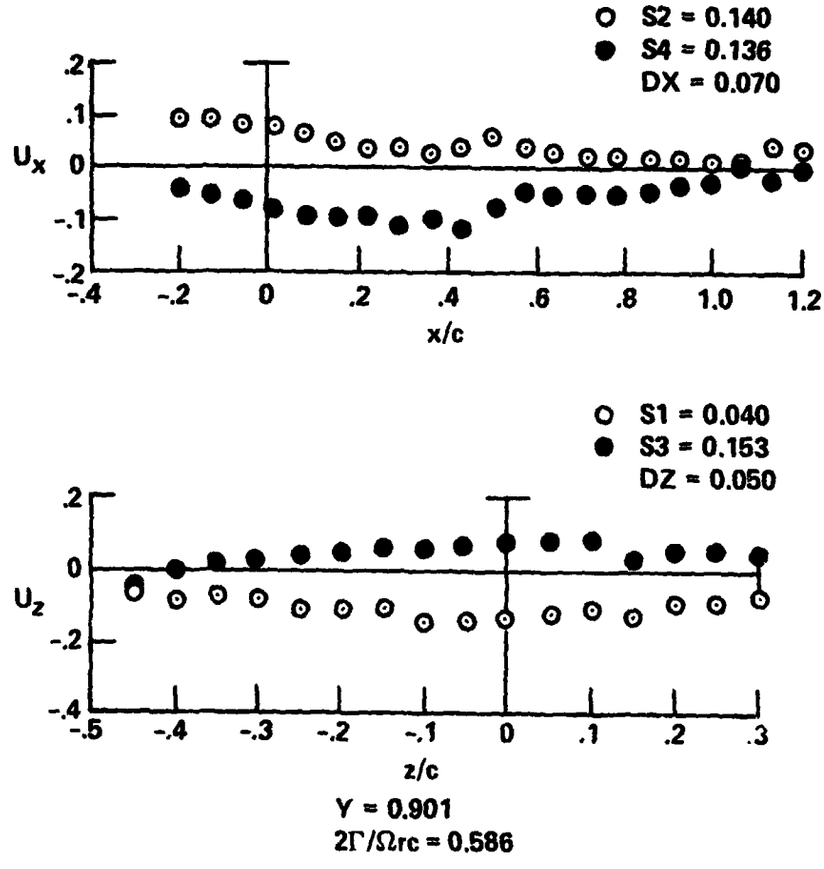

Figure 65.- Flow-field velocities about circulation contour at blade radial station 0.901R for ogee blade tip.

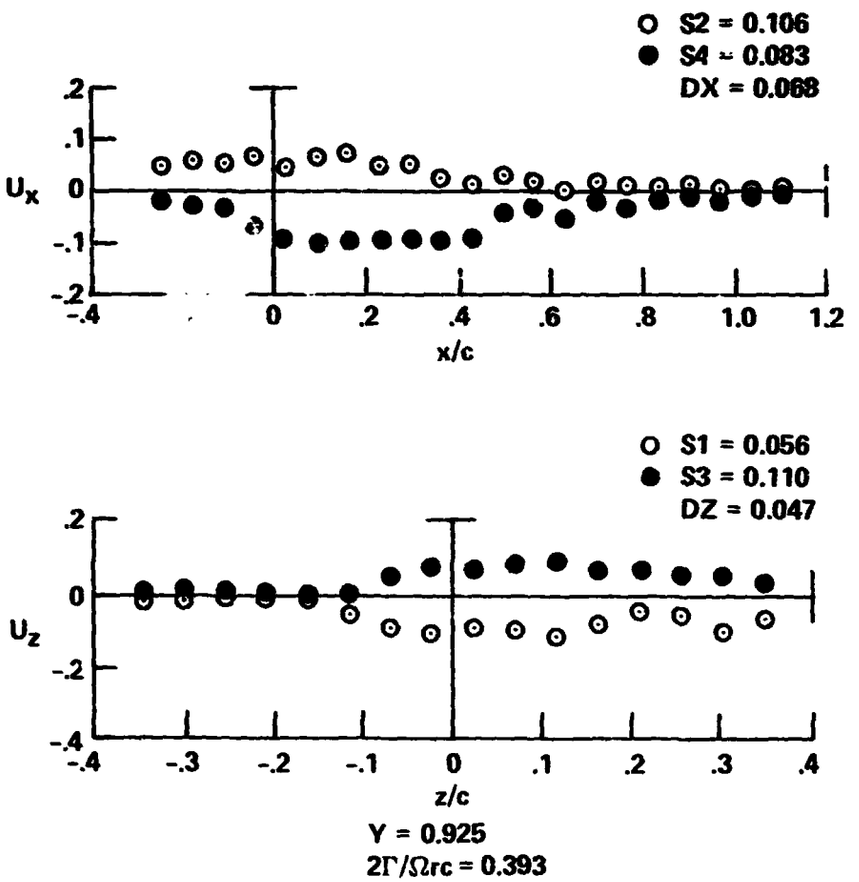

Figure 66.- Flow-field velocities about circulation contour at blade radial station 0.925R for ogee blade tip.

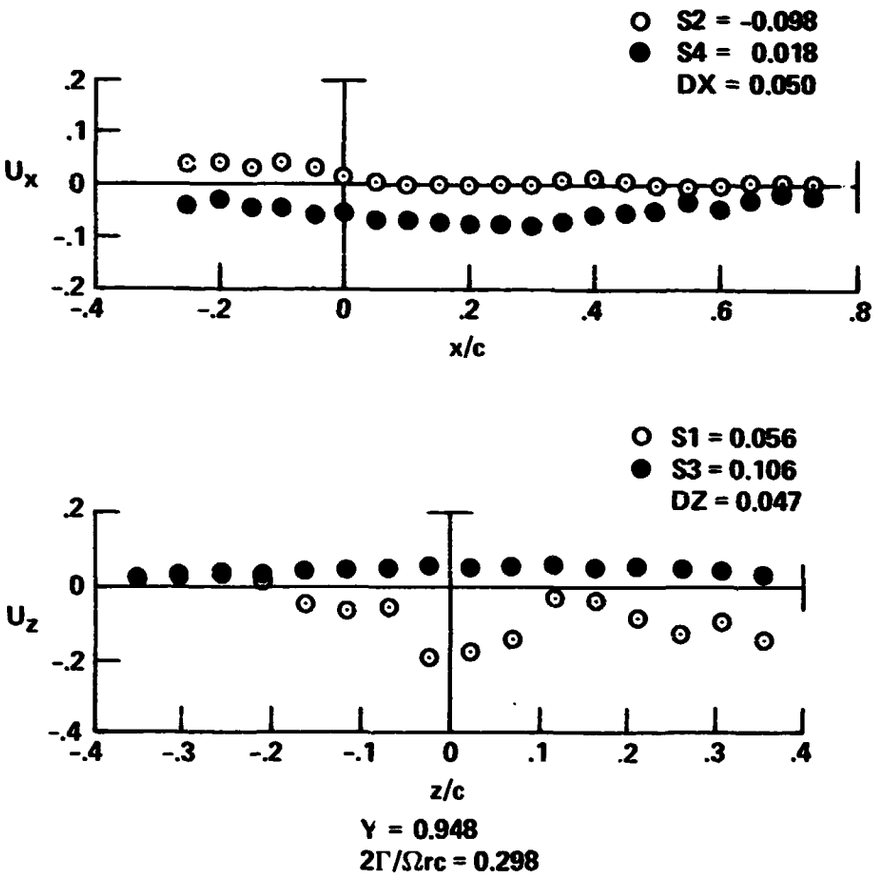

Figure 67.- Flow-field velocities about circulation contour at blade radial station 0.948R for ogee blade tip.

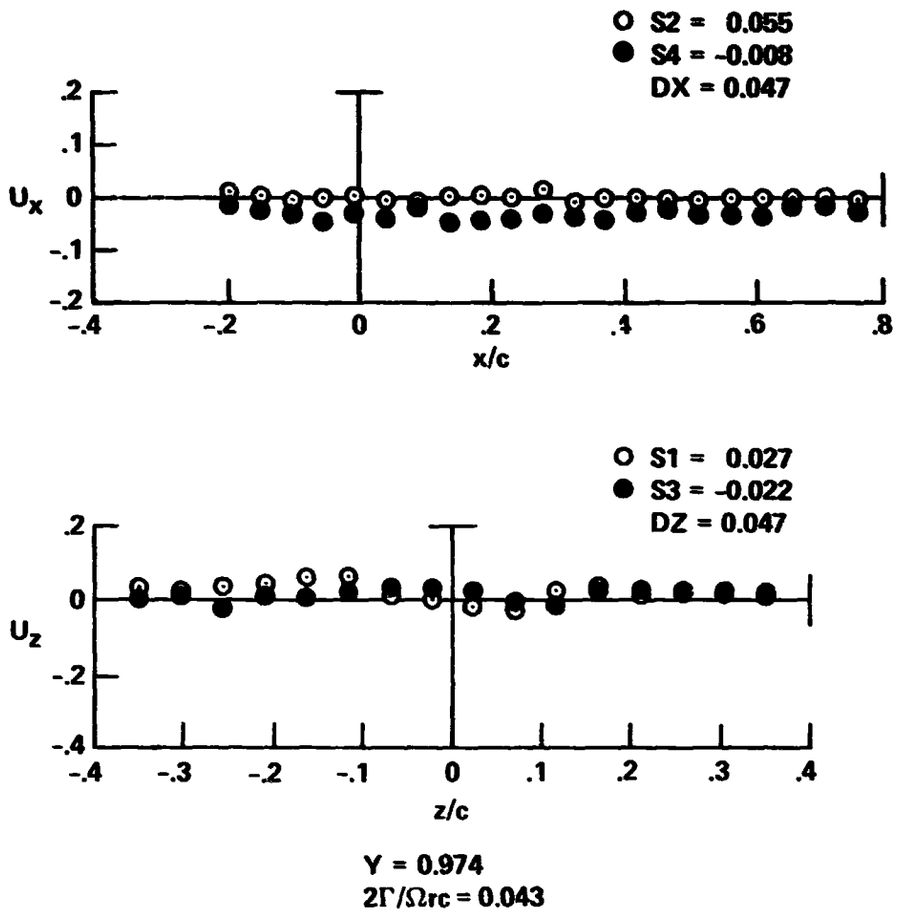

Figure 68.- Flow-field velocities about circulation contour at blade radial station 0.974R for ogee blade tip.

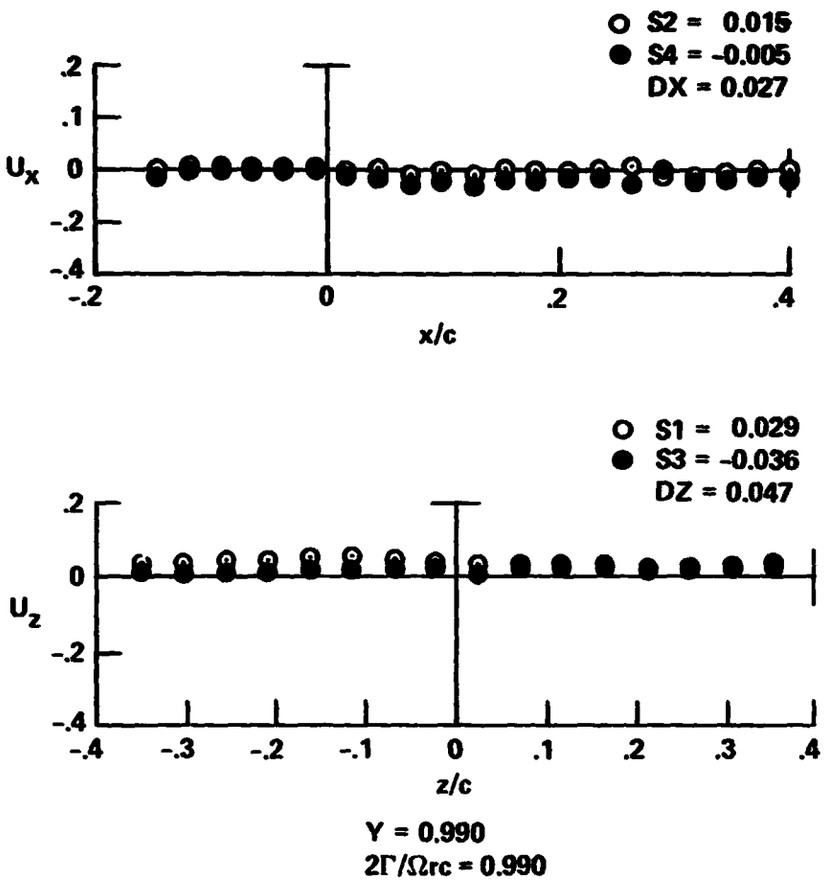

Figure 69.- Flow-field velocities about circulation contour at blade radial station 0.990R for ogee blade tip.

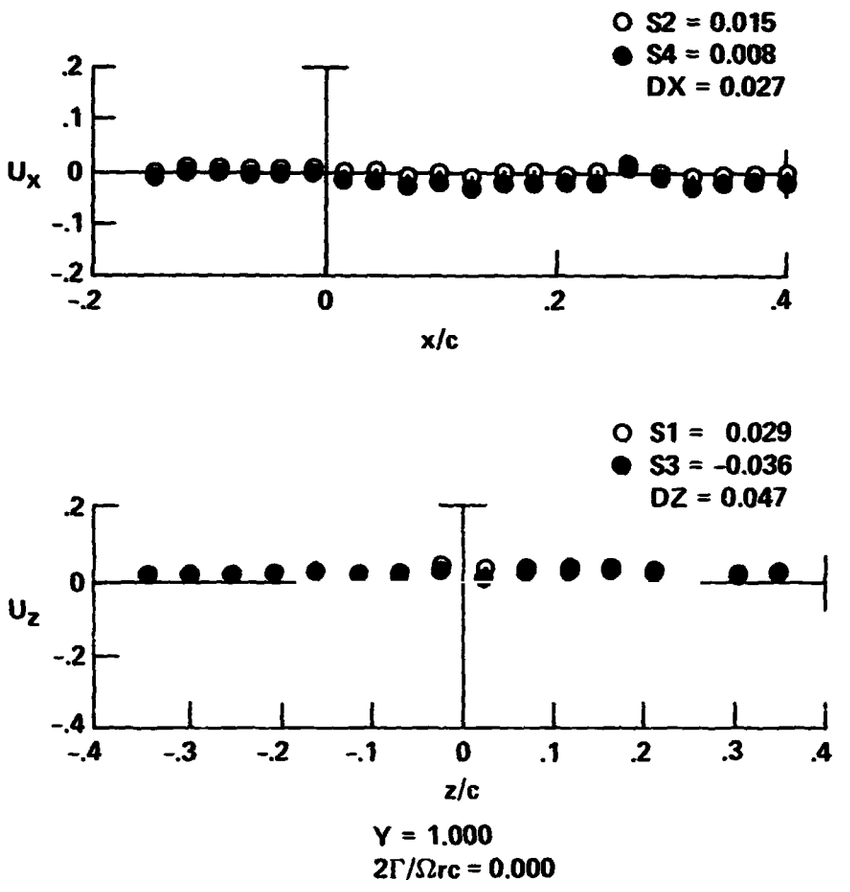

Figure 70.- Flow-field velocities about circulation contour at blade radial station 1.000R for ogee blade tip.